HHS Public Access

Author manuscript

Macromolecules. Author manuscript; available in PMC 2019 December 11.

Published in final edited form as:

Macromolecules. 2018 December 11; 51(23): 9572–9588. doi:10.1021/acs.macromol.8b02059.

Structure of Liquid Coacervates formed by Oppositely Charged Polyelectrolytes

Michael Rubinstein[†], **Qi Liao**[‡], and **Sergey Panyukov**[*]

[†]Departments of Mechanical Engineering and Materials Science, Biomedical Engineering, Physics, and Chemistry, Duke University, Durham, NC 27708, United States (michael.rubinstein@duke.edu)

[‡]Institute of Chemistry of the Chinese Academy of Sciences, Beijing, 100080, P. R., China

[*]P. N. Lebedev Physics Institute, Russian Academy of Sciences, Moscow, 117924, Russia

Abstract

We develop a scaling theory and perform molecular dynamic simulations of weakly interacting coacervates with electrostatic interaction energy per charge less than thermal energy kT. Such liquid coacervates formed by oppositely charged polyelectrolytes can be asymmetric in charge density and number of charges per chain. We predict that these coacervates form interpenetrating solutions with two correlation lengths and two qualitatively different types of conformations of polyelectrolytes with lower and higher charge densities, which are analogous to chain conformations in quasi-neutral and in polyelectrolyte solutions, respectively. Weaker charged chains are attracted to and adsorbed on stronger charged chains forming a screening “coat” around the stronger charged polyelectrolytes. Salt added at lower concentrations screens the repulsion between stronger charged chains, thereby reducing the thickness of the screening coat and resulting in the non-zero net polymer charge in the coacervate. At higher salt concentrations salt screens the attraction between oppositely charged chains, decreasing the coacervate concentration and its polymeric charge density. Thus, we predict a non-monotonic salt concentration dependence of polymeric charge density for asymmetric coacervates. Phase diagram for a mixture of oppositely charged polyelectrolytes at various compositions is proposed for different salt concentrations.

Graphical Abstract

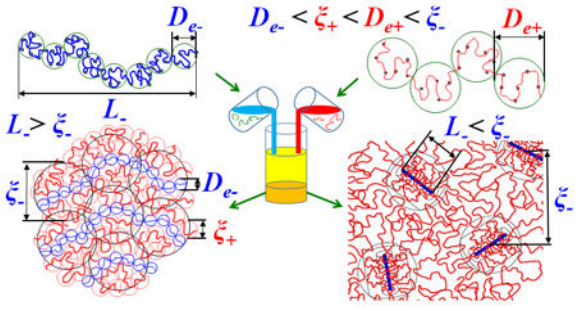

1. Introduction

Mixing oppositely charged polyelectrolytes often results in phase separation into a dense phase, called coacervate, and a dilute solution, containing isolated chains and sometimes small clusters of oppositely charged chains, called complexes. Coacervates consisting of oppositely charged polyelectrolytes are encountered in nature[1] and used in food,[2,3] pharmaceutical[4,5], and other industries.[6,7,8] Even though coacervates formed by mixing oppositely charged polymers have been extensively studied experimentally[9,10,11,12,13] over many decades, there is still no satisfactory description of their structure on a molecular level. Prior theoretical studies of symmetric coacervates include Voorn-Overbeek model[14,15] combining Flory-Higgins with Debye-Hückel theories to incorporate fluctuations in concentrations of charges. Although this model ignores the connectivity of charges on the chains, its predictions are in qualitative agreement with experiment. The effect of connectivity of charges on density fluctuations within the one-loop Random Phase Approximation (RPA) was performed by several groups.[16,17,18,19] This approximation assumes that polymers are weakly perturbed from their ideal Gaussian conformations, and it is, therefore, applicable only for symmetric weakly charged polyelectrolytes. Zhang and Shklovskii[20] mapped out a phase diagram for various salt concentrations, describing the behavior of coacervates and complexes formed by oppositely charged chains with all monomers charged and interacting with each other upon contact with electrostatic energy $\approx kT$, where k is Boltzmann constant and T is absolute temperature. Another proposed mechanism is coacervation driven by the release of condensed counterions[21,22,23]. Complexation of oppositely charged polyelectrolytes has also been investigated by Monte-Carlo[24] and molecular dynamics simulations[25] which demonstrated the formation of different polyelectrolyte complexes accompanied by the counterion release. The field-theoretic simulation methods[26,27,28] made it possible to study complexation and coacervation in symmetric polyelectrolytes with large fluctuations, accounting for inhomogeneities in the polymer concentration. At high concentrations, these methods yield results similar to those obtained within the one-loop approximation.

In this work, we present a scaling theory of the structure of coacervates formed in a solution of polyanions mixed with polycations, containing a different density of charges along polyanion and polycation contours, various charge stoichiometries, and salt concentrations. We demonstrate that chain conformations in coacervates can significantly deviate from ideal (Gaussian) in the case of large asymmetry in charge density charges along polyanion and polycation chain contours. We also generalize the coacervation theory of Shklovskii and coworkers[20] by accounting for polymer flexibility and describing the detailed structure of coacervate and complexes on length scales smaller than the correlation length.

In section 2 we briefly review chain conformations in solutions of positively or negatively charged polyelectrolytes before they are mixed together. In this section, we also review the scaling results for symmetric polyelectrolyte mixtures of polyanions and polycations. In section 3 we develop scaling theory of weak (liquid) coacervates of oppositely charged polyelectrolyte chains. The effect of salt on weak coacervates and the phase diagram of the solution of oppositely charged polyelectrolytes is described in section 4. The details of

molecular dynamics simulations are presented in section 6. The main results are summarized and discussed in section 7.

2. Review of polyelectrolyte solutions and symmetric mixtures of oppositely charged polyelectrolytes

Polyelectrolytes are polymers containing ionizable groups that can dissociate upon dissolution in polar solvents leaving charges on polymer chains and counterions in solutions.[29]

2.1. Review of chain conformations in polyelectrolyte solutions.

A polyelectrolyte chain in a dilute solution can be described at the scaling level as a stretched array of the so-called electrostatic blobs.[29,30] An electrostatic blob is a section of a polyelectrolyte whose energy of electrostatic interaction with an adjacent chain section of similar size and charge is on the order of thermal energy kT. The average number of monomers in an electrostatic blob of a polycation is denoted by g_{e+} with the fraction f_+ of them charged. The charge of an electrostatic blob of this polycation is ef_+g_{e+} and its size in a θ-solvent is $D_{e+} \simeq b_+ g_{e+}^{1/2}$, where b_+ is the Kuhn length[31] of the polycation and e is the elementary charge, see Figure 1. The approximately equal sign "≃" denotes scaling equality up to a coefficient on the order of unity. The electrostatic energy of repulsion between neighboring blobs of a polycation is

$$\frac{(ef_+g_{e+})^2}{\varepsilon b\, g_{e+}^{1/2}} \simeq kT. \quad (1)$$

From the definition of the Bjerrum length l_B – the distance at which two elementary charges in a solvent with dielectric constant ε interact with thermal energy $e^2/(\varepsilon l_B) = kT$, one can express the number of monomers

$$g_{e+} \simeq u_+^{-2/3} f_+^{-4/3} \quad (2)$$

in and size

$$D_{e+} \simeq b_+ u_+^{-1/3} f_+^{-2/3} \quad (3)$$

of an electrostatic blob for a polycation in a θ-solvent in terms of the dimensionless ratio of the Bjerrum length, l_B, and the Kuhn length, b_+, of the polycation

$$u_+ = \frac{l_B}{b_+} = \frac{e^2}{kT\varepsilon b_+}. \quad (4)$$

Similarly, the number of monomers in and the size of an electrostatic blob of a polyanion in a θ-solvent is obtained from the above equations by replacing "+" with "−"

$$g_{e-} \simeq (u_- f_-^2)^{-2/3} \quad (5)$$

$$D_{e-} \simeq b_-(u_- f_-^2)^{-1/3} \quad (6)$$

and denoting the dimensionless ratio of Bjerrum and Kuhn lengths for the polyanion by $u_- = l_B/b_-$. We consider here polyelectrolytes in a θ-solvent, while the results for a good solvent are summarized in Appendix A.

A typical conformation of polyanion chains with $N_- > g_{e-}$ monomers in a dilute solution without added salt is a linear array of N_-/g_{e-} electrostatic blobs[29,30], due to the long range electrostatic repulsion, see Figure 1. The contour length of this array is equal to the end-to-end distance of the polyelectrolyte chain in a dilute salt-free θ-solution

$$L_- \simeq D_{e-}\frac{N_-}{g_{e-}} \simeq \frac{b_-^2 N_-}{D_{e-}} \quad (7)$$

up to the logarithmic corrections.[29,30] The conformations of these chains in salt-free semidilute polyanion solutions are linear arrays of electrostatic blobs on length scales up to correlation length, defined as the average distance between the nearest monomers on neighboring chains

$$\xi_- \simeq D_{e-}\frac{g_-}{g_{e-}}, \quad (8)$$

where g_- is the number of monomers per correlation volume of size ξ_-. The charge ef_-g_- of the polyelectrolyte section of size ξ_- is completely compensated by counterions within this correlation volume, so that the semidilute solution is on average electroneutral on this correlation length scale ξ_-, as well as on larger length scales. A polyanion chain on larger length scales is a random walk of stretched chain sections of size ξ_- with root-mean-square end-to-end distance[29,30]

$$R_- \simeq \xi_-(N_-/g_-)^{1/2}. \quad (9)$$

The correlation length ξ_- of a semidilute polyelectrolyte θ-solution decreases with increasing polymer concentration $\bar{c}_-$ as[29,30]

$$\xi_- \simeq (b_- \bar{c}_-)^{-1/2}(u_- f_-^2)^{-1/6} \quad (10)$$

The osmotic pressure of a polyelectrolyte solution is positive and is dominated by counterions. For salt-free solutions, it is on the order of kT per counterion – the van't Hoff law $\Pi = kT\bar{c}_- f_-$. The properties of dilute and semidilute solutions of polycations are similar to the corresponding polyanion solutions (replace "−" by "+" in the above equations). At higher concentrations of polycations

$$\bar{c}_+ > c_{0+} \simeq b_+^{-3}(u_+ f_+^2)^{1/3}, \quad (11)$$

the correlation length of the polyelectrolyte solution is smaller than the size of the electrostatic blob. Such solutions are called quasi-neutral with chain conformations almost ideal on all length scales in θ-solvents.

2.2. Review of symmetric mixtures of oppositely charged polyelectrolytes.

We consider coacervates formed by complexation of oppositely charged polyelectrolytes in a θ-solvent for uncharged backbones, while the results for a good solvent are presented in Appendix A. In this section, we briefly discuss scaling predictions for symmetric polyelectrolyte mixtures of polyanions and polycations, which are analogous to symmetric block polyampholytes.[32,33,34] By symmetric, we mean polyelectrolytes with the same electrostatic blob size $D_{e+} = D_{e-}$ and, therefore, the same number density of charges along the array of electrostatic blobs of polyanions and polycations, $\gamma_+ = \gamma_-$, where

$$\gamma_- \simeq \frac{f_- g_{e-}}{D_{e-}} \simeq (D_{e-} l_B)^{-1/2} \simeq \frac{1}{b_-}\left(\frac{f_-}{u_-}\right)^{1/3}. \quad (12)$$

and the same expression for γ_+ with "−" replaced by "+". Note that symmetric coacervates could have different degrees of polymerization of polycations and polyanions $N_+ \neq N_-$ and different polymeric charges $N_+ f_+ \neq N_- f_-$. We require symmetry of electrostatic blob sizes and of the resulting line charge densities (Eq. 12), but not necessarily of the degrees of polymerization of chains. The electrostatic blobs, that repel the same sign neighboring blobs with energy kT, attract the oppositely charged blobs of the same size and charge with energy kT. This attraction of oppositely charged blobs in a solution of oppositely charged polyelectrolytes leads to their precipitation into a coacervate (Figure 1).

In the absence of salt, the coacervate has to be electroneutral with the same number density of positive and negative charges. Even though there is the same number of positive and negative blobs in the coacervate, the oppositely charged blobs are more likely to be close to each other because of lower electrostatic energy and higher statistical weight of these configurations. The resulting net attraction is balanced by the short-range repulsion (three-body in a θ-solvent or two-body in a good solvent) that stabilizes coacervate at equilibrium

concentration and zero osmotic pressure, corresponding to the dense packing of electrostatic blobs. Note that the monomer number density of polyanions and polycations in a symmetric coacervate could be different as long as the number density of monovalent charges is the same

$$f_+\bar{c}_+ \simeq \frac{f_+ g_{e+}}{D_{e+}^3} \simeq \frac{1}{l_B^{1/2} D_{e+}^{5/2}} \simeq \gamma_+^5 l_B^2 = \gamma_-^5 l_B^2 = f_-\bar{c}_- \quad (13)$$

with the same equilibrium concentration of charges as in each of the blobs. Thus, the monomer concentrations of polycations and polyanions are reciprocally proportionally to the fractions of charged monomers on the chains $\bar{c}_+/\bar{c}_- = f_-/f_+$ and will only be the same if the fractions of charged monomers are identical $f_+ = f_-$.

3. Weak (liquid) coacervates

Consider the asymmetric coacervate with different number densities of charges along the chains $\gamma_+ \neq \gamma_-$. For definiteness, we assume that polyanions have higher linear charge number density along the array of their electrostatic blobs (Eq. 12) than polycations

$$\gamma_- > \gamma_+ . \quad (14)$$

In this case, polyanions create a higher electric field (see Figure 2a) that attracts polycations and forces them to adsorb on a polyanion forming a screening coat around it (Figure 2b). The attraction of polycations within this coat to the polyanion is stabilized by the short-range (three-body in a θ-solvent or two-body in a good solvent) repulsion between polycations.

The coacervate can be divided into cells consisting of stronger charged polyanions at their centers and compensating coats of weaker charged polycations. Each such cell is overall electroneutral, and therefore, the electric field at the boundary between neighboring cells is zero. Nevertheless, these cells attract each other electrostatically. Since electrostatic interactions decay with the distance between charges, the attraction of a polyanion to the coat of the neighboring cell at typical distance $k\xi_- < \xi_-$ is stronger than its repulsion from the polyanion in the center of this cell at the distance ξ_-, where $1/2 < k < 1$. In addition to this electrostatic attraction, there is an attraction between neighboring cells induced by the entropic elasticity of polycations bridges stretched between regions of the attractions of neighboring polyions. Therefore, the neighboring coats are stitched together by shared polycation chains, different parts of which are attracted to the corresponding polyanions (see Figure 2c). Both electrostatic attraction and bridging are compensated by the short-range repulsion between and within polycation coats and thus, result in the overall zero osmotic pressure of the coacervate.

The unique property of asymmetric coacervates formed by oppositely charged polyelectrolytes with unequal charge densities $\gamma_+ < \gamma_-$ is that they form two interpenetrating

polymeric liquids characterized by two corresponding correlation length: ξ_+ for polycations and ξ_- for polyanions. The correlation length of the polycation "coat" around polyanions, ξ_+, is determined by the local balance of electrostatic attraction of polycations to polyanions and short-range repulsion between polycations. The average distance between sections of neighboring polyanions, the correlation length ξ_-, is the thickness of the polycation coat at which the electro-neutrality of the coacervate is established.

In salt-free solution we distinguish two cases sketched in Figure 3:

a) the semidilute case for long polyanions with the length L_- of the arrays of their electrostatic blobs (Eq. 7) larger than correlation lengths ξ_-, resulting in the coacervates with overlapping polyanion chains, considered in section 3a. We will show that this case corresponds to $L_- > D_{e-}$ $(D_{e+}/D_{e-})^{9/8}$ in a θ-solvent (see Eq. 25 below).

b) the dilute case for shorter polyanions with $L_- < \xi_-$, discussed in section 3b, corresponds to coacervates with spherically symmetric compensating coats on length scales between L_- and ξ_-.

Note, that we distinguish these two cases based on the size L_- (Eq. 7) of polyanion chains with higher charge density in dilute salt-free polyelectrolyte solution relative to the polyanion correlation length ξ_- of coacervate and not to the polycation size, which can be either larger or smaller than L_-. For simplicity, we assume that both polyanions and polycations have the same Kuhn length, $b_+ = b_- \equiv b$, and therefore, dimensionless ratios of Bjerrum to Kuhn lengths are also the same, $u_+ = u_- = l_B/b \equiv u$.

3a Weak (liquid) coacervates with long stronger charged polyelectrolytes – double-semidilute interpenetrating solution.

If the stronger charged polymer (say polyanion) is much larger than its electrostatic blob $L_- \gg D_{e-}$, the electric field around it felt by the polycation screening coat has cylindrical symmetry, see Figure 2a. The electrostatic energy of attraction between a polyanion with f_-N_- charges and its compensating polycation coat of equal and opposite total charge and thickness $\xi_- < L_-$ is

$$F_e \simeq kTl_B\gamma_- f_- N_- \ln(\xi_-/\xi_+) . \quad (15)$$

Here ξ_+ is a minimal radius of the polycation coat to be described in more details below, see Eq. (20). Expression (15) can be interpreted as the energy $Q^2/(2C)$ of a cylindrical capacitor of thickness ξ_- with the charge $Q = ef_-N_-$ and the capacitance $C \simeq \epsilon L_-/\ln(e\xi_-/\xi_+)$. This attraction is balanced by the osmotic repulsive energy of the polycation coat containing f_-N_- compensating charges and therefore f_-N_-/f_- monomers in the coat volume $L_-\xi_-^2$ with the average polycation concentration in the coacervate $\bar{c}_+ \simeq f_- N_-/(f_+ L_-\xi_-^2)$. The osmotic free energy of repulsion between polycations compensating the charge of a single polyanion in volume $L_-\xi_-^2$ in a θ-solvent with the third virial coefficient $\sim b^6$ is

$$F_{os} \simeq kTb^6\bar{c}_+^3(L_-\xi_-^2) \simeq kT\frac{b^4}{\xi_-^4}\frac{f_-^{5/3}}{f_+^3}\frac{N_-}{u^{2/3}} \quad (16)$$

Here we used relation (7) between L_- and N_-. Minimizing the sum of electrostatic (Eq. 15) and osmotic (Eq. 16) free energies per polyanion

$$F = F_e + F_{os} \simeq kTf_-N_-\left[l_B\gamma_-\ln\left(\frac{\xi_-}{\xi_+}\right) + \frac{b^4}{\xi_-^4}\frac{f_-^{2/3}}{f_+^3u^{2/3}}\right] \quad (17)$$

with respect to ξ_-, one obtains the width of the coat – the polyanion correlation length

$$\xi_- \simeq b\frac{f_-^{1/12}}{f_+^{3/4}u^{1/3}} \simeq D_{e+}\left(\frac{D_{e+}}{D_{e-}}\right)^{1/8} \quad \text{for } L_- > \xi_-. \quad (18)$$

Here we used Eqs. (3) and (6) for D_{e+} and D_{e-}. The average polycation number density in the coacervate is

$$\bar{c}_+ \simeq \frac{f_-N_-/f_+}{L_-\xi_-^2} \simeq \frac{f_+^{1/2}f_-^{1/6}u^{1/3}}{b^3} \simeq \frac{1}{b^2D_{e+}}\left(\frac{D_{e+}}{D_{e-}}\right)^{1/4} \quad \text{for } L_- > \xi_- \quad (19)$$

Our prediction in Eq. (19) is verified by the coarse-grained molecular dynamics simulations of θ-coacervates formed by asymmetric oppositely charged polyelectrolytes (see section 6 for the details of the simulations). In Figure 4 we plot $\bar{c}_+\sigma^3/f_+^{1/2}$ as a function of normalized Bjerrum length l_B/σ, where σ is the simulation monomer size. The plot confirms the scaling model prediction that the ratio $\bar{c}_+/f_+^{1/2}$ collapses the simulation data onto a master curve (see Eq. 19) for polycations with different fractions of charged monomers f_+ between 3/61 and 7/61 for the same fraction f_- = 1/2 of charged monomers along the polyanions. This master curve is well fit by the power law function (dashed line in Figure 4) $\bar{c}_+\sigma^3/f_+^{1/2} = 0.6(l_B/\sigma)^{0.4}$. The slope 0.4 of the master curve on the double logarithmic plot is slightly larger than its asymptotic value 1/3 predicted by the scaling model $\bar{c}_+/f_+^{1/2} \simeq l_B^{1/3}f_-^{1/6}b^{-10/3} \sim l_B^{1/3}$.

The number of monomers g_+ in the correlation volume ξ_+^3 of the polycation coat is determined by the close-packing condition, $g_+ \simeq \bar{c}\xi_+^3$. Conformations of polycation chains on the length scales up to this correlation length are Gaussian, $g_+ \simeq (\xi_+/b)^2$, since the correlation length ξ_+ is smaller than the size of the electrostatic blob D_{e+}, and the polycation solution is in a quasi-neutral regime with $\bar{c}_+ > \bar{c}_{0+}$ (see Eq. 11). Equating these expressions

for g_+, we find that the corresponding correlation length is reciprocally proportional to the concentration, as expected in the quasi-neutral regime in a θ-solvent[31]

$$\xi_+ \simeq \frac{1}{\bar{c}_+ b^2} \simeq \frac{b}{u^{1/3} f_+^{1/2} f_-^{1/6}} \simeq D_{e+}\left(\frac{D_{e-}}{D_{e+}}\right)^{1/4} \quad (20)$$

where we used expression (19) for $\bar{c}_+$. For this equilibrium value of the monomer concentration $\bar{c}$ $\gamma_+ \neq \gamma_- \simeq \bar{c}_+$, the energy of the electrostatic attraction of the polycation section of the size ξ_+ containing $f_+ g_+$ positive charges to the polyanion with linear charge number density γ_- is on the order of thermal energy $kTl_B\gamma_- f_+ g_+ \simeq kT$. These polycation sections of size ξ_+ sterically repel each other with the energy $kTb^6\bar{c}_+^3\xi_+^3 \simeq kT$.

The average concentration of positive charges in the asymmetric coacervate is

$$f_+\bar{c}_+ \simeq \frac{f_+ g_+}{\xi_+^3} \simeq \frac{1}{l_B^{1/2} D_{e+}^{5/2}}\left(\frac{D_{e+}}{D_{e-}}\right)^{1/4} \quad (21)$$

Note that for symmetric coacervate with $D_{e+} = D_{e-}$ this equation for the concentration of charges reduces to Eq. (13).

The sizes of electrostatic blobs D_{e+} of polycations and D_{e-} of polyanions determine the multiscale structure of the asymmetric θ-coacervate

$$D_{e-} < \xi_+ \simeq D_{e+}\left(\frac{D_{e-}}{D_{e+}}\right)^{1/4} < D_{e+} < \xi_- \simeq D_{e+}\left(\frac{D_{e+}}{D_{e-}}\right)^{1/8} \quad \text{for } L_- > \xi_- \quad (22)$$

with three important length scales. The smallest length scale D_{e-} is related to the strongest interactions – intramolecular electrostatic repulsions of charges along the polyanions. The next length scale – the correlation length of the polycation coat, ξ_+, corresponds to the balance of electrostatic attraction of polycations to polyanions and short-range non-electrostatic repulsion between polycations. The largest length scale, ξ_-, is the distance between polyanions at which the electroneutrality of the coacervate is achieved.

Thus, asymmetric liquid coacervate consists of two interpenetrating polymer solutions, each with its own correlation length and qualitatively different chain conformations (Figure 5a). These conformations are similar to conformations of pure polyanion and pure polycation solutions with corresponding polymer concentrations $\bar{c}_+$ and $\bar{c}_-$. Higher charge density chains (polyanions) with $L_- > \xi_-$ adopt the conformations similar to polymer conformations in semidilute polyelectrolyte solutions. This observation is supported by a good agreement between structure factors of polyanions in the coacervates and in the pure polyanion solutions, see Figure 5b.

The largest of the three scales we are discussing in Eq. (22) is the correlation length of polyanions that determines the position of the maximum of the polyanion structure factor $S(q)$ at wavevector $q \simeq 1/\xi_-$, see Figure 5b. Different sets of data in this figure correspond to different strengths of electrostatic interactions, characterized by the Bjerrum length l_B. Increasing the strength of the electrostatic attraction requires a stronger short-range repulsion between polycations to balance this attraction at higher concentrations of a thinner coat. The corresponding decrease of the coat thickness ξ_- with the Bjerrum length l_B predicted by Eq. (18) can be seen in Figure 5b as a shift in the position of the maximum of the structure factor $S(q)$ to higher wavevectors $q \simeq 1/\xi_-$.

On length scales smaller than the correlation length ξ_-, polyanion conformations both in coacervates and semidilute polyelectrolyte solutions are linear arrays of electrostatic blobs of size D_{e-} (see the lower set of points in Figure 6 with a slope approaching −1 with increasing Bjerrum length). On length scales larger than the correlation length ξ_-, polyanion conformations both in coacervates and in semidilute polyelectrolyte solutions are random walks with chain size

$$R_- \simeq \xi_- \left(\frac{N_-}{g_-}\right)^{1/2} \simeq bN_-^{1/2}\left(\frac{D_{e+}}{D_{e-}}\right)^{9/16} \quad \text{for } L_- > \xi_-, \quad (23)$$

where g_- is the number of polyanion monomers in the correlation volume ξ_-^3

$$g_- \simeq g_{e-}\frac{\xi_-}{D_{e-}} \simeq g_{e-}\left(\frac{D_{e+}}{D_{e-}}\right)^{9/8} \quad \text{for } L_- > \xi_-. \quad (24)$$

The validity of this semidilute description requires polyanions in coacervates to be above the overlap with each other, $N_- > g_-$, which is the same condition as $L_- > \xi_-$ corresponding to

$$N_-/g_{e-} = L_-/D_{e-} > (D_{e+}/D_{e-})^{9/8}. \quad (25)$$

Note that polyanion chain size becomes that of a random walk $R_- \approx bN_-^{1/2}$ in symmetric θ-coacervates with $D_{e+} = D_{e-}$, but increases in asymmetric coacervates with the asymmetry factor D_{e+}/D_{e-}, see Eq. (23).

Since both intra- and intermolecular electrostatic repulsions between polycations are too weak to affect their conformations, the polycation form-factor can be approximated by the Debye function, see upper sets of points and solid line in Figure 6. Thus, polycations adopt random conformations on all length scales in a θ-coacervate with chain size

$$R_+ \simeq bN_+^{1/2}, \quad (26)$$

as expected for the quasi-neutral solution with $\bar{c}_+ > c_{0+}$.

The similarity between polyanions in coacervates and polyelectrolyte solutions extends beyond chain conformations. Salt-free polyelectrolyte solutions have a characteristic peak in the structure factor $S(q)$. Stronger charged polyanions in the coacervate exhibit similar strong correlations manifested in their structure factor, see Figure 7. The role of lower charge density chains (polycations) in the coacervate is similar to the role of counterions in polyelectrolyte solutions – to screen the charge of strongly charged chains. The difference between the polyelectrolyte solutions and the coacervates is that the behavior of free counterions is dominated by their entropy and therefore, the osmotic pressure of salt-free polyelectrolyte solutions is $\sim kT$ per counterion.[29] The compensating charges in the coacervates reside on the lower charge density chains with significantly reduced translational entropy. The short-range non-electrostatic repulsion between the weaker charge density polycations compensates their electrostatic attraction to the stronger charge density polyanions and reduces the osmotic pressure of the coacervate to zero. This interpenetrating double-semidilute coacervate structure is unique and leads to a number of unusual thermodynamic and dynamic mechanical properties.

Note that the above scaling picture is approximate and ignores a weak variation of the polycation concentration with distance r from the polyanion. Indeed, the charges on polycations adjacent to a polyanion partially screen its electric field and polycations at a larger distance r away from the polyanion feel a weaker electrostatic attraction towards it. This weaker attraction at larger distances requires a weaker stabilizing short-range repulsion between polycations and correspondingly, lower concentration $c_+(r)$. Thus, the concentration of screening polycation coat is expected to slowly decrease with the distance r from the polyanion.[35] (see Figure 7). This figure also demonstrates that increasing the electrostatic attraction with the Bjerrum length l_B results in the polycation coat with a higher concentration $c_+(r)$ and stronger short-range repulsion.

In Appendix B we calculate the concentration profile $c_+(r)$ of polycations by solving the Poisson equation for the dependence of electrostatic potential around a polyanion on the distribution of polycation charges $ef_+c_+(r)$ and by balancing the electrostatic and short-range osmotic forces on polycation segments. We show that this concentration profile of polycations around the oppositely charged rod can be approximated by

$$c_+(r) \simeq \bar{c}_+ \frac{[\ln(\xi_-/r)]^2}{1 + 0.95[\ln(\xi_-/r)]^{3/2}} \quad (27)$$

where $\bar{c}_+$ is the average concentration of polycations estimated by the scaling model (Eq. 19). This prediction (lines in Figure 7 with the fitting parameters presented in Table 1) agrees well with the results of coarse-grained molecular dynamics simulations of $M_+ = 33$ polycation chains consisting of $N_+ = 41$ monomers each with a low fraction of charged monomers $f_+ = 3/41$ adsorbed on a fully charged ($f_- = 1$) rod-like polyanion containing 99 charged monomers (symbols in Figure 7) in a simulation box with size L = 99σ equal to the

length of the linear array of 99 monomers, and with periodic boundary conditions in the direction of this array, thus forming an infinite straight line of negative charges.

3b Weak (liquid) coacervates with short strongly charged polyelectrolytes – dilute-semidilute solution.

The polyanions with the contour length L_- of the linear array of electrostatic blobs (Eq. 7) smaller than the correlation length ξ_- do not overlap with each other. The symmetry of the electric field around each of these polyanions becomes spherical on the length scales $L_- < r < \xi_-$ (Figure 3b). The energy of electrostatic attraction between a polyanion with the net charge ef_-N_- and the polycation screening coat of thickness ξ_- with a charge of the same magnitude and opposite sign, is

$$F_e \simeq -kTl_B\frac{(f_-N_-)^2}{\xi_-} \quad (28)$$

This electrostatic attraction of polycations to polyanion is balanced by the short-range repulsion between polycations. The free energy of three-body repulsion between f_-N_-/f_+ polycation monomers with an average concentration

$$\bar{c}_+ \simeq f_-N_-/(f_+\xi_-^3) \quad (29)$$

in the screening volume ξ_-^3 is

$$F_{os} \simeq kTb^6\bar{c}_+^3\xi_-^3 \simeq kTb^6\frac{f_-^3}{f_+^3}\frac{N_-^3}{\xi_-^6}, \quad (30)$$

where b^6 is the third virial coefficient in a θ-solvent. Minimization of the free energy per polyanion

$$F = F_e + F_{os} \simeq kT(f_-N_-)^2\left[-\frac{l_B}{\xi_-} + \frac{b^6}{\xi_-^6}\frac{f_-N_-}{f_+^3}\right] \quad (31)$$

with respect to ξ_- results in the size of the screening coat – the polyanion correlation length

$$\xi_- \simeq b\left(\frac{f_-N_-}{f_+^3u}\right)^{1/5} \text{ for } L_- < \xi_- \quad (32)$$

Substituting this expression for polyanion correlation length into equation (29) for polycation concentration, we find

$$\bar{c}_+ \simeq b^{-3} u^{3/5} (N_- f_+^2 f_-)^{2/5} \quad (33)$$

In Appendix B we show that the balance of electrostatic attraction of polycations to the polyanion and the short-range three-body repulsion leads to the polycation concentration profile

$$c_+(r) \simeq \frac{(u f_+ f_- N_-)^{1/2}}{r^{1/2} b^{5/2}} \text{for } L_- < r < \xi_- . \quad (34)$$

in the outer spherical region of the screening coat. The symmetry of the electric field at shorter distances from a polyanion $r < L_-$ is still cylindrical and the structure of the polycation coat around a polyanion at these smaller length scales is similar to the case described above (Eq. 27) with the average polycation density $\bar{c}_+ \simeq b^{-3} f_+^{1/2} f_-^{1/6} u^{1/3}$ (Eq. 19).

4. Liquid coacervates in the presence of salt

Addition of salt screens the electrostatic interaction on the length scale of Debye screening length

$$r_D = (8\pi l_B c_s)^{-1/2} \quad (35)$$

where c_s is the concentration of a monovalent salt (e.g. *NaCl*). In the presence of salt, the net charge of polyions does not have to be zero. Below we start from describing coacervates with optimal composition, at which the Gibbs free energy per unit volume of polycations and polyanions are equal $\bar{c}_+ f_+ \mu_+ = \bar{c}_- f_- \mu_-$ and μ_+ and μ_- are polycation and polyanion chemical potentials per charge, and $\bar{c}_+$ and $\bar{c}_-$ are concentrations of polycations and polyanions in the coacervate.

4.1 At low salt concentration

with large Debye length $r_D > \xi_-$, the salt practically does not affect the coacervate structure. This low salt regime corresponds to salt concentrations

$$c_s < c_{s,l} \simeq \frac{f_+^{3/2} f_-^{-1/6}}{b^3 u^{1/3}} \quad (36)$$

In this regime, the optimal composition corresponds to electroneutral coacervate with equal concentrations of charges of polycations and polyanions, $f_+ \bar{c}_+ = f_- \bar{c}_-$ and equal chemical potentials per charge $\mu_+ = \mu_-$.

4.2 At intermediate salt concentrations

in an asymmetric coacervate with intermediate Debye radius $\xi_+ < r_D > \xi_-$, salt ions screen repulsion on length scales larger than the Debye length, whereas attraction predominates on a smaller length scale $\xi_+ < r_D$. Therefore, the thickness of the polycation coat ξ_-^S decreases with increasing salt concentration from its salt-free value ξ_-, see Figure 8 a. The charge q_+^s of polycations in the correlation cell with size ξ_-^s also decreases with increasing salt concentration and is smaller than the charge q_-^s of a polyanion in this cell by the factor $q_+^s/q_-^s \simeq (\xi_-^s/\xi_-)^d < 1$. Here $d = 2$ for a cylindrically-symmetric cell with $L_- > \xi_-^s$ and $d = 3$ for a spherically-symmetric cell with $L_- > \xi_-^s$. The attraction force between polyanion charge q_-^s and polycations in the neighboring cell with the charge q_+^s at the effective distance $k\xi_-^s < \xi_-^s$ is $l_B q_+^s q_-^s/(k\xi_-^s)^2 \exp(-k\xi_-^s/r_D)$. The repulsion force between polyanions in neighboring cells $l_B(q_-^s)^2/(\xi_-^s)^2 \exp(-\xi_-^s/r_D)$ is weaker than the attraction force as long as the cell size ξ_-^S is logarithmically larger the Debye screening length, $\xi_-^s \gtrsim r_D \ln(\xi_-/r_D)$.

Below, we drop the logarithmic corrections and limit our discussion to the scaling relations. Within this approximation the correlation length ξ_-^s decreases with increasing salt concentrationfrom its salt-free value ξ_- (see Eq. 18)

$$\xi_-^s \simeq \begin{cases} \xi_- & \text{for} \quad c_s < c_{s,l} \\ r_D \approx (l_B c_s)^{-1/2} & \text{for} \quad c_{s,l} < c_s < c_{s,h} \end{cases} \tag{37}$$

see Figure 9. Here the upper boundary $c_{s,h}$ of the intermediate salt concentration regime corresponds to the Debye radius on the order of polycation correlation length, $r_D \simeq \xi_+$, Eq. (20):

$$c_{s,h} \simeq \frac{f_+ f_-^{1/3}}{b^3 u^{1/3}} \simeq \left(\frac{f_-}{f_+}\right)^{1/2} c_{s,l} \tag{38}$$

The coacervate structure is determined by the balance of attraction of polycations to polyanions and steric repulsion between polycation chains. This balance is unaffected by the salt at distances from polyanions shorter than the Debye screening length. Therefore, in the intermediate salt regime, the coacervate structure at these length scales $r < r_D$ around polyanion is almost the same as in the salt-free case.

Polycation chains are Gaussian in a θ-solvent since their intramolecular electrostatic repulsion on the scale ξ_+ is weaker than kT. Their concentration profile depends on whether

Debye length is smaller or larger than the size L_- of polyanions in a dilute salt-free polyelectrolyte solution (Eq. 7):

4.2a Coacervates with a long stronger charged polyelectrolyte, $L_- > \xi_-$ in the intermediate salt regime.

In this regime, polyanions overlap with each other since their size is larger than their correlation length ξ_-^s. Polyanions conformations in such a coacervate are similar to conformations of the same polyanions in the semidilute polyelectrolyte solution with the same concentration c_-, see section 3a. The salt screens both repulsion and attraction between charged chains, thereby reducing the separation between polyanions to the Debye length r_D. The polycation concentration in the coacervate remains almost the same as in the salt-free case, see Eq. (19), due to unchanged interactions on the length scales smaller than the Debye length. The correlation length ξ_+ of polycations is also unaffected by the salt as long as it is smaller than the Debye screening length r_D in the intermediate salt concentration regime, see Figure 9.

The net charge of chains inside the optimal coacervate is no longer zero and is controlled by the polyanion charges. The number density of polyanion charges is the net charge f_-N_- of one chain divided by the volume per chain $L_-r_D^2$. Using Eq. (7) we find that it increases linearly with salt concentration c_s (see Figure 10)

$$f_-\bar{c}_- \simeq \frac{f_-D_{e-}}{b^2r_D^2} \simeq u^{2/3}f_-^{1/3}c_s, \qquad \text{at} \quad c_{s,l} < c_s < c_{s,h} \tag{39}$$

4.2b Coacervates with a short stronger charged polyelectrolyte, $L_- < \xi_-$, in the intermediate salt regime.

This intermediate salt regime can be divided into two sub-regimes. The first sub-regime with $L_- < r_D < \xi_-$ corresponds to dilute/semidilute coacervate with non-overlapping polyanions. With increasing salt concentration, the separation between polyanions is reduced to the Debye length r_D. In this sub-regime polymer conformations and the structure of the coacervate are similar to those in the salt-free case, see section 3. The polycation concentration $c_+(r)$, Eq. (19), in a cylindrical zone $\xi_+ < r < L_-$ close to the polyanion is almost uniform, and decreases with distance r from the polyanion, Eq. (34), in the outer spherical zone for $L_- < r < r_D$. In this first sub-regime with $L_- < r_D < \xi_-(c_{s,l}^{\text{sph}} < c_s < c_s^*$ with $c_{s,l}^{\text{sph}} \simeq c_{s,l}^{4/5}(c_s^*)^{1/5}$ and $c_s^* \simeq (l_BL_-^2)^{-1})$ the coacervate concentration is dominated by polycations in the outer spherical zone and increases with salt concentration as $\bar{c}_+ \simeq c_+(r_D)$ (see Figure 10):

$$\bar{c} \simeq \bar{c}_+ \simeq \begin{cases} b^{-3}u^{3/5}(f_+^2f_-N_-)^{2/5} & \text{for} \quad c_s < c_{s,l}^{\text{sph}} \\ b^{-9/4}u^{3/4}(f_+f_-N_-)^{1/2}c_s^{1/4} & \text{for} \quad c_{s,l}^{\text{sph}} < c_s < c_s^* \end{cases} \tag{40}$$

where Eq. (34) was used.

The total charge of all chains is dominated by polyanions and increases with increasing salt concentration c_s, approaching the charge of polyanions at high salt concentration. The density of total charge on chains increases with salt concentration as $f_-\bar{c}_- \simeq f_-N_-/r_D^3$ (see Figure 10):

$$f_-\bar{c}_- \simeq \begin{cases} b^{-3}u^{3/5}f_+^{9/5}(f_-N_-)^{2/5} & \text{for} \quad c_s < c_{s,l}^{\text{sph}} \\ f_-N_-(l_Bc_s)^{3/2} & \text{for} \quad c_{s,l}^{\text{sph}} < c_s < c_s^* \end{cases} \tag{41}$$

In the second intermediate salt sub-regime, the Debye length is shorter than the polyanion size, $\xi_+ < r_D < L_-$, and polyanions overlap with each other forming double-semidilute coacervate discussed in section 4.2a. Salt dependence of polymer concentration and of the net charge on chains in this sub-regime is the same as in double-semidilute coacervates (see section 4.2 and Eq. 39).

4.3 In the high salt regime with $c_s > c_{s,h}$,

the screening length is smaller than the correlation length of polycations, $r_D < \xi_+$, and the structure of the optimal coacervate for both cases with longer ($L_- > \xi_-$) and shorter ($L_- < \xi_-$) stronger charged polyanions is identical. In this high salt regime, electrostatic attraction between polycation and polyanion sections of size r_D. Therefore, the interaction between positively and negatively charged chains within coacervate can be described as an effective two-body attraction between elementary charges with a negative second virial coefficient $-l_Br_D^2$. This virial coefficient determines the free energy density $-kTl_Br_D^2(f_+c_+)(f_-c_-)$ of electrostatic attraction between positive charges with concentration f_+c_+ and negative charges with concentration f_-c_-. This free energy is on the order of thermal energy kT on the scale of polyanion correlation length ξ_-^s,

$$kTl_Br_D^2f_+f_-c_+c_-(\xi_-^s)^3 \simeq kT\,. \tag{42}$$

The attraction between polycations and polyanions is stabilized by the third virial repulsion between polycations with energy density $kT/(\xi_+^s)^3$ and two-body intermolecular repulsion between polyanions $kT/(\xi_-^s)^3$, which are on the same order of magnitude in the optimal coacervate. Therefore, the correlation lengths of both polycations and polyanions within the optimal coacervate are the same

$$\xi \simeq \xi_+^s \simeq \xi_-^s \simeq \frac{b^4c_s}{f_+^{3/2}f_-^{1/2}}, \qquad \text{at} \quad c_s > c_{s,h} \tag{43}$$

see Figure 9.

The structure of the optimal coacervate is the dense packing of correlation blobs of size ξ. Half of these blobs contains polycation sections, while the other half contains polyanion sections. This structure on the scale of the correlation length is similar to the structure of the "scramble egg" symmetric coacervate with equal charge densities, see Ref.[36]. Conformations of polycations are Gaussian in a θ-solvent for uncharged backbone for both asymmetric and symmetric coacervates. Polyanion conformations are Gaussian for symmetric coacervates while they are non-Gaussian in asymmetric coacervates and depend on salt concentration.

The conformations of polyanions in an asymmetric coacervate in the high salt regime with Debye length $r_D < \xi_+$ are similar to conformations of the same chains in the polyelectrolyte solution with the same salt and polymer concentration.[37] Polyanion conformations in both cases for $r_D > D_{e-}$ can be described as a linear array of electrostatic blobs of size D_{e-} on length scales up to the Debye screening length r_D and as a self-avoiding walk of Debye volumes on length scales between r_D and the correlation length ξ. On length scales larger than ξ, polyanion conformations in both asymmetric coacervate and polyelectrolyte solution are random walks of correlation volumes.

At even higher salt concentration with Debye screening length smaller than polyanion electrostatic blob size, $r_D < D_{e-}$, polyanions are ideal on scales larger than the correlation blob ξ, Eq. (43), as well as on length scales smaller than the size $\xi_T \simeq D_{e-}^3/r_D^2$ of the thermal blob. The conformations are self-avoiding walks of thermal blobs of size ξ_T on intermediate length scales, $\xi_T < r < \xi$. Note that the thermal blob size ξ_T increases proportionally to the salt concentration similarly to the correlation length ξ, Eq. (43). This implies, that the range of the self-avoiding behavior $\xi/\xi_T \simeq (f_-/f_+)^{3/2}$ is independent of salt concentration. In the optimal symmetric coacervate with $f_+ = f_-$, the size of the thermal blob is on the order of the correlation length, $\xi_T \simeq \xi$, and both polycations and polyanions are Gaussian in a θ-solvent. Also note, that linear dependence of the correlation length on salt concentration $\xi \sim c_s$ is valid for both high salt sub-regimes with Debye screening length $D_{e-} < r_D < \xi_+$ and $r_D < D_{e-}$ only for Flory exponent $\nu = 3/5$. In Appendix C we show that the salt dependence of the screening length is slightly modified for $\nu = 0.588$.

The concentration of coacervate is dominated by polycations in all salt regimes. In the double-semidilute regime with $L_- > \xi_-$ the concentration of the optimal coacervate is

$$\bar{c} \simeq \bar{c}_+ \simeq \frac{1}{b^2 \xi_+} \simeq \begin{cases} b^{-3} u^{1/3} (f_+^3 f_-)^{1/6} & \text{for} \quad c_s < c_{s,h} \\ b^{-6} (f_+^3 f_-)^{1/2} c_s^{-1} & \text{for} \quad c_s > c_{s,h} \end{cases} \tag{44}$$

It is almost salt independent in both low and intermediate salt regimes for $c_s < c_{s,h}$ with Debye length $r_D > \xi_+$. In the high salt regime for $c_s > c_{s,h}$ with $r_D < \xi_+$, salt screens attraction between polyanions and polycations and the coacervate concentration decreases reciprocally with increasing salt concentration, see Eq. (44) and Figure 10.

The polyanion concentration $\bar{c}_-$ varies nonmonotonically with salt concentration c_s and is lower than the polycation concentration:

$$\bar{c}_- \simeq \begin{cases} b^{-3}u^{1/3}f_+^{3/2}f_-^{-5/6} & \text{for} \quad c_s < c_{s,l} \\ u^{2/3}f_-^{-2/3}c_s & \text{for} \quad c_{s,l} < c_s < c_{s,h} \\ b^{-6}f_+^2 c_s^{-1} & \text{for} \quad c_s > c_{s,h} \end{cases} \tag{45}$$

The net number density of charges on chains in the optimal coacervate is non-zero and is dominated by the stronger charged polyanions $f_-\bar{c}_- - f_+\bar{c}_+ \simeq f_-\bar{c}_-$ at salt concentrations above $c_{s,l}$. This charge density varies non-monotonically with salt concentration: it increases linearly with c_s in the intermediate salt regime, see Eq. (39), and decreases reciprocally with increasing salt concentration c_s in the high salt regime, see Figure 10. This non-monotonic behavior disappears for the optimal symmetric coacervate with $f_+ = f_-$ because there is no intermediate salt regime with $\xi_+ < r_D < \xi_-$, since $\xi_+ \simeq \xi_-$. The net charge density on chains in the symmetric coacervate decreases reciprocally with salt concentration.

In the case of shorter polyanions with $L_- < \xi_-$, there is an additional salt dependence regime for Debye screening length $r_D < L_-$, corresponding to polyanion chains below their overlap. In this regime at a salt concentration $c_s < c_s^* \simeq (l_B L_-^2)^{-1}$, the correlation cell has spherical symmetry with the coacervate concentration and the net charge increasing as 1/4 and 3/2 powers of salt concentration, respectively (Eqs. 40 and 41), see dotted lines in Figure 10.

4.4 Generalized Shklovskii phase diagram.

In the above sections, we studied coacervate with optimal composition, corresponding to equal Gibbs free energy per unit volume of polycations and polyanions, $\bar{c}_+ f_+ \mu_+ = \bar{c}_- f_- \mu_-$. Oppositely charged polyelectrolytes are often mixed with the stoichiometry different from the optimal one. Below we describe the states of such mixtures at different total number fractions of polycation monomers $\phi^{tot} = \bar{c}_+^{tot}/(\bar{c}_+^{tot} + \bar{c}_-^{tot})$ and various salt concentrations c_s, see phase diagram in Figure 11. The thick black lines on this diagram separate a two-phase region from a single-phase region. The dense phase in the two-phase region is the coacervate. Therefore, the thick lines are the boundaries between states with and without the coacervate. The dilute phase could consist of either only free chains or a mixture of free chains and complexes – small aggregates of oppositely charged polyelectrolytes. The complexes can be found in the regions between thin blue lines and red dashed lines in the phase diagram, and thus, can exist in both single and two-phase regions. The single-phase region outside the red dashed line corresponds to a homogeneous mixture of free polyanion and polycation chains with attraction electrostatic energy between them less than kT.

At the green dotted line, the coacervate has an optimal composition with concentrations equal to the total concentrations of the mixture, $\bar{c}_+ = \bar{c}_+^{tot}$ and $\bar{c}_- = \bar{c}_-^{tot}$. In the low-salt solutions, $c_s < c_{s,l}$, the concentrations of polyanion and polycation charges in the optimal coacervate are the same, $f_+\bar{c}_+ = f_-\bar{c}_-$, corresponding to the number fraction of polycation

monomers $\phi_{l,s} = f_-/(f_+ + f_-)$ (see low vertical part of the green dotted line in Figure 11). At higher salt concentrations $c_s > c_{s,l}$, in the optimal coacervate, the total charge of the stronger charged chains (polyanions) is higher than the charge of the weaker charged chains (polycations). In the high-salt regime, $c_s > c_{s,h}$, from Eqs. (44) and (45) the ratio of polyanion and polycation charges in the optimal coacervate reaches its maximal value, $f_-\bar{c}_-/(f_+\bar{c}_+) = (f_-/f_+)^{1/2}$, corresponding to $\phi_{h,s} = f_-^{1/2}/(f_+^{1/2} + f_-^{1/2})$ (upper vertical part of the green dotted line in Figure 11). At intermediate salt concentrations $c_{s,l} < c_s < c_{s,h}$, using Eqs. (44) and (45) we find that the green dotted line, corresponding to the optimal coacervate composition is a hyperbola

$$c_s \simeq c_{s,l}\frac{f_-}{f_+}\left(\frac{1}{\phi} - 1\right), \quad \text{for} \quad \phi_{h,s} < \phi = \phi^{opt} < \phi_{l,s}. \quad (46)$$

This prediction is for double-semidilute coacervates with $L_- > \xi_-$, while for a coacervate with shorter polyanions, $L_- < \xi_-$, there is an additional regime with spherical symmetry and a slightly different shape of the green dotted curve, $c_s \simeq c_{s,l}[f_-/f_+(1/\phi - 1)]^{4/5}$ for $c_{s,l}^{sph} < c_s < c_s^*$.

In the presence of salt, the coacervate can exist even in mixtures with the composition ϕ^{tot} different from the optimal coacervate composition (dotted green line in Figure 11). In such mixtures, the coacervate composition deviates from the optimal composition, ϕ^{opt}, described above, and in the absence of complexes (between thin blue lines in Figure 11, for $\phi_c' < \phi < \phi_c''$) the coacervate composition coincides with the total mixture composition, $\phi = \phi^{tot}$, see the green line in Figure 12. At larger deviations of the coacervate composition from the optimal one (between thin blue and thick black lines in the phase diagram, for $\phi' < \phi < \phi_c'$ and $\phi_c'' < \phi < \phi''$) the coacervate coexists with complexes. The composition of the coacervate in this part of the two-phase region of the phase diagram is the same as its composition at the thin blue line in Figure 11 at the same salt concentration, see two horizontal blue lines $\phi = \phi_c'$ and $\phi = \phi_c''$ in Figure 12. The coacervate dissolves at the boundary of the two-phase region (thick black lines ϕ' and ϕ“), and the composition of complexes inside the two-phase zone (between thin blue and thick black lines in the phase diagram, for $\phi' < \phi\phi' < \phi < \phi_c'$ and $\phi_c'' < \phi < \phi''$) is given by its value at the phase boundary (thick black line ϕ’ or ϕ“) at the same salt concentration. The relative fractions of polymers in the coacervate and in complexes is determined by the lever rule.[38] The shapes and the locations of boundaries of these regimes (thin blue and thick black lines in Figure 11) are obtained by equating chemical potentials of polyanions per negative charge in the coacervate and in the complex, $\mu_-^{complex} = \mu_-$, and similar equality for polycations, $\mu_+^{complex} = \mu_+$, see Appendix D for details.

The red dash line in phase diagram corresponds to the condition at which the attraction energy per chain is on the order of entropic free energy gain per chain upon dissociation of complexes into individual chains. Note that in the limit of symmetric (with fractions of

charged monomers $f_+ = f_- \approx 1$) strongly interacting (with interaction parameter $u \approx 1$) chains, the details of the molecular structure of the polymer chains are not important, and the phase diagram in Figure 11 approaches the diagram obtained in Ref.[20].

5. Molecular Dynamics Simulations

The molecular dynamics simulations were carried out using the bead-spring model.[39] All beads had mass m and diameter σ and interacted with each other via the truncated and shifted Lennard-Jones (LJ) potential

$$U_{LJ}(r) = \begin{cases} 4\varepsilon_{LJ}\left[\left(\frac{\sigma}{r}\right)^{12} - \left(\frac{\sigma}{r}\right)^{6} - \left(\frac{\sigma}{r_c}\right)^{12} + \left(\frac{\sigma}{r_c}\right)^{6}\right], & r \le r_c \\ 0 & r > r_c \end{cases} \quad (47)$$

where the cutoff distance $r_c = 2.5\sigma$ and the LJ parameter $\varepsilon_{LJ} = 0.30kT$ corresponds to the θ-solvent for uncharged polymers. Beads along the chains were connected by the additional unbreakable finitely extensible nonlinear elastic (FENE) potential $U_{FENE}(r)$

$$U_{\text{FENE}}(r) = -\frac{1}{2}KR_0^2 \ln\left(1 - \frac{r^2}{R_0^2}\right) \quad (48)$$

Here $K = 30\varepsilon_{LJ}/\upsilon^2$ is the spring constant and $R_0 = 1.5\sigma$ is the maximum bond length.

Each polyanion chain consisted of $N_- = 101$ beads with the fraction of charged monomers $f_- = 51/101$ and therefore contained $n_- = 51$ negatively charged beads. Polycation chains consisted of $N_+ = 61$ monomers each, and contained n_+ between 3 and 7 positively charged beads corresponding to fractions of charged monomers $f_+ = \frac{3}{61}, \frac{4}{61}, \frac{5}{61}, \frac{6}{61}, \frac{7}{61}$. Charged monomers were monovalent and evenly spaced along the chain backbones with both ends of each chain charged. The periodic simulation box contained $M_- = 20$ polyanion chains for $n_+ = 3,4,5,6$ and $M_- = 21$ polyanion chains for $n_+ = 7$. The number M_+ of polycation chains was determined by the overall electroneutrality condition of the simulation box $M_+ = M_- n_-/n_+$ in the range between $153 \le M_+ \le 340$.

The simulations were carried out with an implicit solvent modelled by a dielectric medium with the dielectric constant ε. All charged beads interacted with each other via the unscreened Coulomb potential

$$U_{\text{Coul}}(r) = kTl_B\frac{z_i z_j}{r} \quad (49)$$

where z_i is the charge valence of the i-th particle (+1 for positive and −1 for negative beads). The Bjerrum length l_B determines the strength of the electrostatic interactions and was varied in the interval $0.01\sigma \le l_B \le 20\sigma$. The electrostatic interactions between all charges in

the simulation box and all of their periodic images were computed by the particle mesh Ewald (PME) algorithm implemented in the LAMMPS software packages.[40,42] All stochastic molecular dynamics simulations[41] were carried out using the Large-scale Atomic/Molecular Massively Parallel Simulator (LAMMPS) parallel MD code.[42] The equations of motion were integrated using the velocity-Verlet algorithm with a time step $\delta t = 0.01\,\tau_{LJ}$, where the Lennard-Jones time is $\tau_{LJ} = (m\sigma^2/\varepsilon_{LJ})^{1/2}$. For all simulations, the constant temperature was maintained by weakly coupling the system to a Langevin heat bath,[43] with a damping constant $\Gamma = 1.0 m/\tau_{LJ}$. The coacervate phase of oppositely charged polyelectrolytes was simulated by setting the osmotic pressure to zero. The Berendsen barostat was used to simulate the equilibrium coacervate at constant pressure $p = 0$.[44] Initial states for chains was chosen from the ensemble of self-avoiding random walk configurations within a periodic cubic box with boundary length L. The approach to equilibrium was quantified by monitoring the relaxation of end-to-end vectors of chains, as well as the fluctuations of the volume of the coacervates. The duration of the equilibration after the coacervate volume reached its final value was chosen to be 2-10 relaxation times of the end-to-end vectors of chains. The structure factor of polyanions at wavevector $\boldsymbol{q}$ was calculated as

$$S(q) = \frac{1}{N}\left\langle \varphi(\boldsymbol{q})\varphi(-\boldsymbol{q})\right\rangle, \quad (50)$$

where the Fourier transform of the monomer concentration profile $\varphi(\boldsymbol{q}) = \sum_{i=1}^{N} \exp(i\boldsymbol{q}\cdot\boldsymbol{r}_i)$, with monomer coordinates $\boldsymbol{r}_i$ for all polyanion chains in the periodic simulation box, and brackets $\langle\ldots\rangle$ denote the ensemble average over chain conformations.

The form factor of a chain was calculated as

$$P(q) = \frac{1}{N^2}\left\langle \Sigma_{i,j}\frac{\sin(qr_{ij})}{qr_{ij}}\right\rangle, \quad (51)$$

where r_{ij} is the distance between i-th and j-th chain monomers. Form factors of polycations were fitted by the Debye function (see Figure 6)

$$P(q) = \frac{2}{Q^2}(e^{-Q} - 1 + Q), \quad (52)$$

with $Q = q^2R_g^2$ resulting in the mean square radius of gyration $R_g^2 = 21.7 \pm 0.5\,\sigma^2$ in good agreement with $R_g^2 = 20.6\,\sigma^2$ obtained directly from the chain coordinates.

6. Conclusions

We presented a scaling theory of the structure of liquid coacervate formed by oppositely charged polyelectrolytes with electrostatic interaction energy between two elementary charges less than the thermal energy kT. We consider relatively weakly charged polyelectrolytes with the line density of charges below the counterion condensation threshold, $\gamma < \gamma_M = 1/l_B$. In the case $\gamma > \gamma_M$, the counterion condensation results in saturation of the effective line density of charges at the Manning value γ_M. In either case, mixing of weakly-interacting polyelectrolytes does not lead to a counterion release upon formation of liquid coacervates because electrostatic energy per charge is less than thermal energy kT. The intramolecular electrostatic interactions in dilute solutions of only polyanions or only polycations are described by the so-called electrostatic blobs of size D_{e-x} or D_{e+} respectively, see the upper part of Figure 1. Sections of a polyelectrolyte chain of size equal to the electrostatic blob size repel neighboring sections of the same chain with electrostatic energy on the order of kT. Conformations of polyanion or polycation chains in their respective dilute solutions before mixing with no added salt can be described as linear arrays of their corresponding electrostatic blobs of size D_{e-} or D_{e+}. Mixing of oppositely charged polyelectrolytes can result in:

- **i.** single-phase homogeneous solution containing charged complexes and/or isolated chains or
- **ii.** two-phase solutions with a coacervate and a dilute phase containing complexes and/or isolated chains

The structure of the coacervate formed upon mixing polyanion and polycation solutions is determined by the balance of electrostatic attraction between oppositely charged polyelectrolytes and short-range repulsion. In the symmetric case with $D_{e-} = D_{e+} = D_e$, the coacervate is a dense packing of these electrostatic blobs with neighboring oppositely charged blobs of size D_e attracting each other with energy on order kT, see the lower right part of Figure 1. This attraction is stabilized by the short-range non-electrostatic repulsion with energy on the same order kT between all chain sections of size D_e.

In an asymmetric case with stronger intramolecular electrostatic repulsion within the polyanion, $D_{e-} < D_{e+}$, the structure of the coacervate is more complex. Such a coacervate is characterized by two correlation lengths, ξ_+ and ξ_-, of polycations and polyanions, respectively (Eqs 20 and 18). Conformations of both positive and negative polyions in coacervates are similar to their conformations in their respective solutions containing polyelectrolytes of only one sign, with the same concentrations ($\bar{c}_+$ and $\bar{c}_-$) and the same correlation lengths (ξ_+ and ξ_- as in the coacervate. Since the polycation correlation length ξ_+ is smaller than its electrostatic blob size, D_{e+}, the corresponding polycation solution with chains of only one sign is quasi-neutral and is analogous to a semidilute solution of uncharged polymers with correlation length ξ_+ with ideal chain conformations in a θ-solvent. The polyanion correlation length ξ_- is larger than its electrostatic blob size, D_{e-}, resulting in its stretched conformations on length scales between its electrostatic blob size D_{e-} and correlation length ξ_- due to strong intermolecular repulsion, similar to their conformations in pure polyanion solutions, see Figure 5.

Weaker charged polycation chains adsorb on stronger charged polyanions forming screening "coats" around them. The electrostatic attraction of polycations to polyanions is balanced by the short-range repulsion between sections of polycations of size ξ_+ with energy on the order of thermal energy kT. This short-range repulsion between polycations is stronger than the electrostatic repulsion between them, since $\xi_+ < D_{e+}$.

The attraction of polycations to a polyanion slowly decreases in strength with increasing distance from the polyanion within the polycation "coat" resulting in a slow (logarithmic) decrease of coat concentration (see Eqs. 27 and B4a-B7a). The thickness of this coat is the inter-polyanion correlation length ξ_-, and in the salt-free mixtures, it is determined by the length scale at which the polycation "coat" compensates the polyanion charge. This compensating polycation coat of coacervates plays the role of counterions of semidilute polyanion solution with the essential difference of negligible translational entropy and important short-range inter-polycation repulsion balancing electrostatic attraction and reducing the osmotic pressure of coacervates to zero (see Figure 5). The order of interactions from strongest to weakest corresponding to the order of length scales from shortest to largest is $D_{e-} < \xi_+ < D_{e+} < \xi_-$.

Key predictions of our scaling model, such as:

- **i.** the dependence of polycation concentration $\bar{c}_+$ in the optimal coacervate on the fraction f_+ of polycation monomers that are charged (Figure 4),
- **ii.** an equivalence of the structure factors of polyanions in the coacervate and in the semidilute polyelectrolyte solution with the same concentration $\bar{c}_-$ (Figure 5),
- **iii.** ideal conformations of weakly charged polycations and stretched conformations of strongly charged polyanions in the coacervate, obtained from their form factors (Figure 6),
- **iv.** the concentration profile in polycation screening coat around strongly charged polycation (Figure 7),

were confirmed by the molecular dynamics simulations.

The coacervate can be isolated from the supernatant, and the coacervate concentration can be increased by partially removing (evaporating) the solvent. In this case, both polyanion and polycation concentrations increase proportionally to each other, while the corresponding correlation lengths are not proportional to each other. The polyanion correlation length ξ_- is reciprocally proportional to the square root of the coacervate concentration, $\xi_- \sim 1/\sqrt{\bar{c}}$, whereas the polycation correlation length ξ_+ decreases reciprocally with coacervate concentration, $\xi_+ \sim 1/\bar{c}$. This implies that the ratio of the two correlation lengths ξ_-/ξ_+ increases as the square root of coacervate concentration, thereby increasing the coacervate asymmetry.

At low salt concentrations with Debye length longer than polyanion correlation length (for $r_D > \xi_-$), the structure of the coacervate is almost the same as in the salt-free case. For intermediate salt concentration with Debye length between the two correlation lengths, $\xi_+ < r_D \xi_-$, the thickness of the polycation coat is reduced and becomes on the order of the Debye

radius r_D. The coacervate concentration is dominated by polycations, and in the high salt regime, it decreases inversely proportionally with increasing salt concentration.

The net charge of the chains of such optimal coacervate in the presence of salt is no longer zero and approaches the net charge of polyanions with decreasing the Debye length. The net charge density of chains in the coacervate varies non-monotonically with salt concentration. It is almost zero at low salt concentrations $c_s < c_{s,l}$, increases linearly with c_s in the intermediate salt regime, $c_{s,l} < c_s < c_{s,h}$, and decreases reciprocally with increasing salt concentration c_s in the high salt regime, $c_s > c_{s,h}$, see Figure 10.

The above predictions for asymmetric coacervate structure and qualitatively different chain conformations of polyanions and polycations (see Figure 5 and Figure 6) can be tested by scattering experiments. The overall coacervate structure factor can be directly measured by small angle X-ray scattering, while the form-factors of polyanions and polycations can be obtained by small angle neutron scattering using the index matching technique[45]. The predicted dependence of the coacervate concentration on fractions f_+ and f_- of charged monomers can be experimentally tested by either varying pH for weak polyelectrolytes, or by synthesizing and measuring concentrations of strong polyelectrolytes with different charge fractions. This dependence is predicted to be different for relatively long and short polyanion chains (Eqs. 19 and 33).

Acknowledgements

We acknowledge financial support from National Science Foundation under Grants DMR-1121107 and EFMA-1830957, the National Institutes of Health under Grants P01-HL108808, R01-HL136961, and 5UH3HL123645, and the Cystic Fibrosis Foundation. This work was supported by grants from National Science Foundation, National Institutes of Health and Cystic Fibrosis Foundation. Q.L. has received the financial support for this work from the National Natural Science Foundation of China under Grants 21574139.

Appendix A General solvent

Below we present main results obtained for general scaling exponent ν describing different solvent conditions for uncharged backbone. The case $\nu = 1/2$ corresponds to a θ-solvent, described in details in the main text with the same equation numbers, and the case $\nu = 0.588$ describes the corresponding athermal solvent:

$$g_{e+} \simeq (u_+ f_+^2)^{-1/(2-\nu)} \quad (2a)$$

$$D_{e+} \simeq b_+ (u_+ f_+^2)^{-\nu/(2-\nu)} \quad (3a)$$

$$g_{e-} \simeq (u_- f_-^2)^{-1/(2-\nu)} \quad (5a)$$

$$D_{e\_} \simeq b_{\_}(u_{\_}f_{\_}^2)^{-\nu/(2-\nu)} \quad (6a)$$

$$L_{\_} \simeq b_{\_}^{1/\nu} N_{\_}/D_{e\_}^{1/\nu - 1} \quad (7a)$$

$$\xi_{\_} \simeq (b_{\_}\bar{c}_{\_})^{-1/2}(u_{\_}f_{\_}^2)^{-(1-\nu)/(2(2-\nu))} \quad (10a)$$

$$\xi_{+} \simeq D_{e+}(D_{e\_}/D_{e+})^{\nu/2} \quad (20a)$$

$$f_{+}\bar{c}_{+} \simeq l_B^{-1/2} D_{e+}^{-5/2}(D_{e\_}/D_{e+})^{(3\nu-1)/2} \quad (21a)$$

$$\bar{c}_{+}b^3 \simeq [f_{+}(f_{\_}^{\nu}u)^{1/(2-\nu)}]^{3\nu-1} \quad (19a)$$

$$\xi_{\_} \simeq D_{e+}(D_{e+}/D_{e\_})^{(2-3\nu)/4} \quad (18a)$$

$$D_{e\_} < \xi_{+} \simeq D_{e+}(D_{e\_}/D_{e+})^{\nu/2} < D_{e+} < \xi_{\_} \simeq D_{e+}(D_{e+}/D_{e\_})^{(2-3\nu)/4} \quad (22a)$$

$$R_{\_} \simeq bN_{\_}^{1/2}(D_{e+}/D_{e\_})^{3(2-\nu)/8} \quad (23a)$$

$$g_{\_} \simeq g_{e\_}(D_{e+}/D_{e\_})^{3(2-\nu)/4} \quad (24a)$$

$$\xi_{\_} \simeq b(N_{\_}f_{\_})^{\frac{2-3\nu}{4-3\nu}} u^{-\frac{3\nu-1}{4-3\nu}} f_{+}^{-\frac{3\nu}{4-3\nu}} \quad (18a)$$

Appendix B Polycation concentration profile

Consider a single polyanion surrounded by a polyanion coat. In case of cylindrical symmetry ($d = 2$), a long polyanion with length $L_- < \xi_-$ is modeled as a uniformly charged cylinder of radius $r_0 \simeq D_{e-}$ with linear charge density γ_-. In case of spherical symmetry ($d = 3$), a short polyanion with length $L_- < \xi_-$ is modeled as the charge $e\gamma_- L_-$ inside a sphere of radius $r_0 \simeq L_-$. The electrostatic potential $\phi(r)$ in the polycation coat, at $r_0 \le r \le \xi_-$, is determined by the Poisson equation

$$\frac{d^2\phi}{dr^2} + \frac{d-1}{r}\frac{d\phi}{dr} = \frac{4\pi}{\varepsilon} e f_+ c_+ \quad \text{(B1)}$$

within the mean-field approximation. The boundary condition at the charged cylindrical surface at $r = r_0$ is

$$r\frac{d\phi}{dr}\bigg|_{r=r_0} = -\frac{2e}{\varepsilon}\gamma_- \quad \text{(B2)}$$

The density c_+ of polycation monomers is found by minimizing the free energy which has both electrostatic and osmotic contributions. In the case of θ-solvent, the osmotic part accounts for the three-body repulsion between monomers, and the c_+-dependent contribution to the free energy is

$$\int \left[-(\mu + e f_+ \phi)c_+ + kTb^6 c_+^3\right] d^3 r \quad \text{(B3)}$$

The chemical potential μ in Eq. (B3) takes into account the normalization of the density c_+ of polycation monomers with their total numer $N_+^{tot} = \int c_+ d^3 r$. Minimizing this free energy with respect to c_+ we find the dependence of monomer concentration $c_+(r)$ of polycations on the electrostatic potential $\phi(r)$:

$$c_+(r) \simeq b^{-3}[\mu_e(r)/kT]^{1/2}, \quad \text{(B4)}$$

The electrochemical potential $\mu_e(r) = \mu + e f_+ \phi(r)$ and the monomer concentration $c_+(r)$ decay to zero at distance $r > \xi_-$ outside the polycation coat.

In the case of cylindrical symmetry $d = 2$, we are looking for the solution of Eqs. (B1) and (B4) in the form

$$\phi(r) = \frac{kT}{e}(4\pi u)^2 b^{-4} f_+^3 \xi_-^4 \chi_2^2 \left[\ln\left(\frac{\xi_-}{r}\right)\right] \quad \text{(B5)}$$

where the dimensionless function $\chi_2(x)$, which determines the dependence of the polycation monomer density on the distance r from the polyanion, is the solution of the equation $\frac{d^2\chi_2^2(x)}{dx^2} = \chi_2(x)e^{-2x}$. Its analytical expression can be found in two limits $x \ll 1$ and $x \gg 1$ (near the surface of the polycation coat and away from it). Joining these solutions for $x \simeq 1$, we can approximate the solution for all $x > 0$ by

$$\chi_2(x) = \frac{x^2}{12(1 + ax^{3/2})}, \quad \text{(B6)}$$

The constant $a \approx 0.95$ is determined from the best fit of the numerical solution of this equation by the function $\chi_2(x)$ given in Eq. (B6), see Figure 13. Substituting this solution into the boundary condition (B2), we get

$$\xi_- \simeq b^{5/4}\gamma_-^{1/4}u^{-1/4}f_+^{-3/4} \quad \text{(B7)}$$

Generalizing the above consideration for the case of a general solvent with scaling exponent ν, we find

$$c_+(r) \simeq b^{-3}[f_+\varphi(r)]^{3\nu - 1} \quad \text{(B4a)}$$

$$\phi(r) = \frac{kT}{e}\left\{ub^{-2}f_+^{3\nu}\xi_-^2\chi_2\left[\ln\left(\frac{\xi_-}{r}\right)\right]\right\}^{1/(2-3\nu)} \quad \text{(B5a)}$$

$$\chi_2(x) = \frac{(2-3\nu)^2}{6\nu}\frac{x^2}{1 + ax^{3\nu}} \quad \text{(B6a)}$$

$$\xi_- \simeq b^{2-3\nu/2}\gamma_-^{1-3\nu/2}u^{(1-3\nu)/2}f_+^{-3\nu/2} \quad \text{(B7a)}$$

Here, the exponent $\nu = 1/2$ in the case of a θ solvent, and $\nu = 0.588$ in the case of a good solvent.

In the case of spherical symmetry ($d = 3$) the solution of Eqs. (B1) and (B4) for a θ-solvent is

$$\phi(r) = \frac{kT}{er}(4\pi u)^2 b^{-4} f_+^3 \xi_-^5 \chi_3^2(r/\xi_-) \quad \text{(B5c)}$$

The dimensionless function $\sigma_3(x)$ is determined by the equation $\frac{d^2\chi_3^2(x)}{dx^2} = \chi_3(x)x^{1/2}$, an approximate solution of which is

$$\chi_3(x) = \frac{(1-x)^2}{12}\frac{1+ax}{1+a} \quad \text{(B6c)}$$

with constant $a \approx 0.35$, see inset in Figure 13. Substituting Eqs. (B5c) and (B6c) into the boundary condition (B2), we reproduce Eqs. (32) for ξ_- and (34) for the concentration profile $c_+(r)$.

Appendix C. High salt regime

Salt ions screen electrostatic interaction at the length scale of the Debye radius r_D, Eq. (35). Charged polymers with their screening salt ion clouds can be represented in the high salt regime $c_s > c_{s,h} = (f_-/f_+)^{1/2} c_{s,l}$ (see Eqs. 36 and 38) by chains of effectively neutral blobs of size r_D, see Figure 8b). The electrostatic interaction energy between polycation blobs of size $r_D < \xi_+$ is less than kT in the high salt regime. Therefore polycations have Gaussian statistics in a θ-solvent on all length scales including the scale of the correlation length $\xi_+ \simeq bg_+^{1/2}$. The number of polycation monomers g_+ on this length scale is determined by the close-packing condition of correlation blobs, $g_+ \simeq c_+\xi_+^3$. Solving these two equation, we find the relation between the polycation concentration $\bar{c}_+$ and the correlation length ξ_+ for the quasi-neutral polyelectrolyte regime in a θ-solvent

$$\bar{c}_+ \simeq \frac{1}{b^2\xi_+} \quad \text{(C1)}$$

This dependence was used in the derivation of Eq. (44). Stronger charged polyanions repel each other, and their statistics depends on the ratio between the Debye radius, Eq. (35), and the electrostatic blob size, Eq. (6). Below, we consider two cases:

High salt regime 1 with $c_{s,h} < c_s < c_{s,t} = c_{s,h}f_-/f_+$.

In this case $D_{e-} < r_D < \xi_+$, and polyanion chains have excluded volume statistics on length scales $r_D < r < \xi_-$ larger than Debye length, but smaller than the correlation length $\xi_- \simeq r_D(g_-/g_D)^{\nu}$. Here g_- and $g_D \simeq g_{e-}(r_D/D_{e-})$ (Eq. 7 for the segment of g_D monomers) are the number of polyanion monomers inside the correlation and Debye volumes, respectively. Since different correlation volumes do not overlap with each other, the polyanion concentration is determined by the dense packing condition of the correlation volumes:

$$\bar{c}_- \simeq g_-/\xi_-^3, \quad \text{(C2)}$$

Substituting the expression for the number of monomer units

$$g_- \simeq g_D\left(\frac{\xi_-}{r_D}\right)^\nu \simeq g_{e-}\frac{r_D}{D_{e-}}\left(\frac{\xi_-}{r_D}\right)^\nu \simeq \frac{D_{e-}r_D}{b^2}\left(\frac{\xi_-}{r_D}\right)^\nu, \quad \text{(C3)}$$

we find the polyanion concentration

$$\bar{c}_- \simeq \frac{D_{e-}}{b^2 r_D^{1/\nu-1}\xi_-^{3-1/\nu}} \quad \text{(C4)}$$

Substituting Eqs. (C1) and (C4) into Eq. (42) for the attraction energy between polycations and polyanions with $\xi \simeq \xi_- \simeq \xi_+$, we find the correlation length

$$\xi \simeq bu^{-\frac{3-5\nu}{6(1-\nu)}}\left(f_+ f_-^{1/3}\right)^{-\frac{\nu}{1-\nu}}(b^3 c_s)^{\frac{3\nu-1}{2(1-\nu)}} \quad \text{for} \quad c_{s,h} < c_s < c_{s,t} \quad \text{(C5)}$$

High salt regime 2 with $c_s > c_{s,t} = c_{s,h}f_-/f_+$.

In this case, the Debye length is smaller than the electrostatic blob of polyanions, $r_D < D_{e-}$. The electrostatic energy of $g_D = r_D^2/b^2$ monomers of the polyanion blob of radius r_D is $\epsilon_D \simeq kTl_B(g_D f_-)^2/r_D \simeq kT(r_D/D_{e-})^3$, and is smaller than thermal energy kT for $r_D < D_{e-}$. A chain segment of the thermal blob size $\xi_T > r_D$ with the number of monomers $g_T = \xi_T^2/b^2$ is Gaussian, and its energy $\epsilon_T \simeq \epsilon_D(g_T/g_D)^{1/2}$ is on the order of kT. Here $(g_T/g_D)^{1/2}$ is the number of pair contacts with energy ϵ_D of electrostatic blobs on the length scale of the thermal blob size ξ_T. From this condition, $\epsilon_T \simeq kT$, we find the number of monomers, $g_T \simeq D_{e-}^6/(b^2 r_D^4) > g_{e-}$, and the size, $\xi_T \simeq b\, g_T^{1/2} \simeq D_{e-}^3/r_D^2 > D_{e-}$ of the thermal blob. On larger length scales, the polyanion has excluded volume statistics and the correlation length becomes

$$\xi_- \simeq \xi_T(g_-/g_T)^\nu \quad \text{for} \quad c_s > c_{s,t} \quad \text{(C6)}$$

Substituting this expression into Eq. (C2), we find the average polyanion concentration

$$\bar{c}_- \simeq \frac{1}{b^{1/\nu}\xi_-^{3-1/\nu}}\left(\frac{D_{e-}^3}{br_D^2}\right)^{2-1/\nu} \quad \text{for} \quad c_s > c_{s,t} \quad \text{(C7)}$$

Substituting Eqs. (C1) and (C7) into Eq. (42), we find the correlation length

$$\xi \simeq \xi_- \simeq \xi_+ \simeq b^4 f_+^{-\frac{\nu}{1-\nu}} f_-^{\frac{3\nu-2}{1-\nu}} c_s \quad \text{(C8)}$$

For the value of Flory exponent $\nu = 3/5$, both expressions (C5) and (C8) turn to Eq. (43). For $\nu = 0.588$, the exponent 0.927 of the c_s-dependence of correlation length in Eq. (C5) only slightly differs from its Flory value of unity.

Appendix D. Chemical potentials and phase diagram

The unique feature of mixtures of oppositely charged polyelectrolytes is the existence of stable complexes consisting of chains of opposite charges. Below we assume that the charge of the polycationic chain significantly exceeds the charge of the polyanionic chain, $N_-f_- \gg N_+f_+$. Consider a complex consisting of a single polyanion chain with N_-f_- elementary charges and n polycation chains with $q_+ = nN_+f_+$ elementary charges. The structure of the complexes is determined from the condition of the equality of polyions chemical potentials in the coexisting phases. In general, the chemical potential per charge is defined as the energy of moving a unit charge to infinity. Since the charges of the complex can be removed only with the corresponding chains, this definition requires a substantial refinement:

The polycation chemical potential is

$$\mu_+^{complex} = \partial F^{complex}(q_+)/\partial q_+ \quad \text{(D1)}$$

where $F^{complex}(q_+)$ is the free energy of the complex. Since there is only one polyanionic chain per complex, its “removal to infinity” leads to a decrease in the number k of complexes by unity. In order to define the polyanion chemical potential, consider the difference of free energies of configurations of $k + 1$ complexes with q'_+ positive charges and k complexes with q_+ charges:

$$(k+1)F^{complex}(q'_+) - kF^{complex}(q_+) \quad \text{(D2)}$$

These configurations have the same total number of positive charges, $(k+1)q'_+ = kq_+$, and the difference of N_-f_- negative charges. Dividing Eq. (D2) by N_-f_-, in the limit $k \gg 1$ we find the polyanion chemical potential per unit negative charge:

$$\mu_{-}^{complex} = \frac{F^{complex}(q_{+}) - q_{+}\mu_{+}^{complex}}{N_{-}f_{-}} \quad \text{(D3)}$$

Low salt regime with $c_s < c_{s,l}$.

In this case, the charge with concentration $\bar{c}_{+}f_{+} - \bar{c}_{-}f_{-}$ is distributed in the volume V of the coacervate, and its free energy density is

$$F/V \simeq kTl_B r_D^2(\bar{c}_{+}f_{+} - \bar{c}_{-}f_{-})^2 + kT\bar{c}_{-}f_{-}l_B\gamma_{-}\ln(\xi_{-}^{s}/\xi_{+}), \quad \text{(D4)}$$

where $l_B r_D^2$ is the effective second virial coefficient, and the second term in Eq. (D4) is the energy of attraction of polycation coat with the radius $\xi_{-}^{s} \simeq \xi_{-}$ to the polyanion, see Eq. (15) and Figure 2b. Differentiating the free energy of the coacervate (D4) with respect to the number of charges, $n_{+} = V\bar{C}_{+}f_{+}$ and $n_{-} = V\bar{C}_{-}f_{-}$, we find its chemical potentials,

$$\begin{aligned} \mu_{+} &\simeq kTl_B r_D^2(\bar{c}_{+}f_{+} - \bar{c}_{-}f_{-}), \\ \mu_{-} &\simeq -kTl_B r_D^2(\bar{c}_{+}f_{+} - \bar{c}_{-}f_{-}) + kTl_B\gamma_{-}\ln(\xi_{-}^{s}/\xi_{+}) \end{aligned} \quad \text{(D5)}$$

Now, consider the cylindrically-shaped complex with the diameter ξ_{-}^{s}, the length L_{-}, and occupying the volume $V \simeq L_{-}(\xi_{-}^{s})^2$, see Figure 14. The free energy of such a complex with polycation charge $q_{+} \simeq \bar{c}_{+}f_{+}V$ is the sum $F^{complex} = F_C + F_V + F_S$ of the Coulomb F_C, volume F_V, and surface F_S terms:

$$F_c \simeq kT\frac{l_B}{L_{-}}(q_{+} - N_{-}f_{-})^2\ln\frac{\min(L_{-}, r_D)}{\xi_{-}^{s}}, \quad \text{(D6)}$$

$$F_V \simeq kTVc_{-}f_{-}l_B\gamma_{-}\ln\left(\frac{\xi_{-}^{s}}{\xi_{+}}\right), \qquad F_S \simeq \sigma\xi_{-}L_{-}$$

Here $\sigma \simeq kT/\xi_{+}^2$ is the surface tension. The chemical potentials of the complex are obtained by substituting this free energy into Eqs. (D1) and (D2).

Below we describe the equilibrium of the coacervate and dilute phase of complexes. Equating the corresponding chemical potentials of the coexisting phases, we find that the Coulomb and the surface contributions are on the same order, $F_c \simeq F_s$, and that the charge of the complex is

$$q_+ - N_- f_- \simeq \pm L_- \left(\frac{\sigma \xi_-}{kTl_B} / \ln \frac{\min(L_-, r_D)}{\xi_-} \right)^{1/2} \quad \text{(D7)}$$

The charge density of the coacervate, coexisting with the complexes is

$$\bar{c}_+ f_+ - \bar{c}_- f_- \simeq \pm \frac{1}{r_D^2} \left(\frac{\sigma \xi_-}{kTl_B} \ln \frac{\min(L_-, r_D)}{\xi_-} \right)^{1/2} \quad \text{(D8)}$$

The sign (−) describes the left region between thick black and thin blue lines in Figure 11, and the sign (+) describes the corresponding right region. The charge of each of these complexes (Eq. D7) is, respectively, lower and higher than the chain charge per polyanion in the coacervate.

At the blue lines in the phase diagram in Figure 11 the concentration of the polyions in the coacervate is the same as the total concentrations, $c_+ = \bar{c}_+^{tot}$ and $c_- = \bar{c}_-^{tot}$. Substituting these equalities into Eq. (D8), we find the number fraction of polycation monomers at the lower part of these two lines:

$$\phi_c' \simeq \frac{1}{2} - \frac{\xi_-^2}{r_D^2} \left(\ln \frac{\min(L_-, r_D)}{\xi_-} \right)^{1/2}, \quad \text{(D9)}$$

$$\phi_c'' \simeq \frac{1}{2} + \frac{\xi_-^2}{r_D^2} \left(\ln \frac{\min(L_-, r_D)}{\xi_-} \right)^{1/2}$$

The fraction of complexes in the dilute phase is increasing upon approaching the thick black lines on the phase diagram in Figure 11 from the two-phase side, while the fraction of coacervate is decreasing and disappears at the phase boundary. At this line, the fraction of polycation charge of the complex is the same as the total fraction of polycation charges in the mixture,

$$\frac{q_+}{N_- f_-} = \frac{\bar{c}_+^{tot} f_+}{\bar{c}_-^{tot} f_-} \quad \text{(D10)}$$

Substituting q_+ from this equation into Eq. (D7), we find the number fraction of polycation monomers on the boundary between one- and two-phase regions on the phase diagram:

$$\phi' \simeq \frac{1}{2} - \left(\ln\frac{\min(L_-, r_D)}{\xi_-}\right)^{-1/2}, \qquad \phi'' \simeq \frac{1}{2} + \left(\ln\frac{\min(L_-, r_D)}{\xi_-}\right)^{-1/2} \tag{D11}$$

Intermediate salt regime with $c_{s,l} < c_s < c_{s,h}$.

The diameter ξ_-^s of the optimal polycation coat in the coacervate (see Figure 8a) can be estimated in this case, from the minimum of the free energy of correlation cells with size ξ_-^s:

$$F \simeq kTl_B\left[\frac{(q_-^s)^2}{L_-}e^{-\xi_-^s/r_D} + \frac{q_+^s q_-^s}{kL_-}e^{-k\xi_-^s/r_D}\right] \tag{D12}$$

with polyanion charge of the complex $q_-^s \simeq \gamma_- L_-$ and polycation charge $q_+^s \simeq \bar{c}_+ f_+ (\xi_-^s)^2 L_-$, giving $\xi_-^{opt} \simeq 2(1-k) r_D \ln(\xi_-/r_D)$. Expanding this free energy near this minimum, we find within the quadratic approximation

$$\Delta F \simeq kTl_B L_- \gamma_-^2 \left(\frac{r_D}{\xi_-}\right)^{2(1+k)} \left(\frac{\xi_-^s - \xi_-^{opt}}{r_D}\right)^2 \simeq kT\frac{l_B}{L_-}\left(\frac{r_D}{\xi_-}\right)^{2(1-k)} \left(q_+ - q_+^{opt}\right)^2 \tag{D13}$$

This expression replaces the first term in Eq. (D4) for the case of intermediate salt concentration. The resulting phase boundaries in Figure 11 in this regime can be approximated by the vertical lines.

High salt regime with $c_s > c_{s,h}$.

All the results obtained in Appendix C for this regime can also be derived from a minimum of the coacervate free energy:

$$F/V = -kTl_B r_D^2 f_+ f_- c_+ c_- + kTb^6 c_+^3 + kT/\xi_-^3 \tag{D14}$$

The first term is the energy of attraction of polyanions and polycations with the second virial coefficient $l_B r_D^2$ per charge, see Eq. (42), the second term is the energy of steric 3-body repulsion of polycations, and the last term is the energy of the effective repulsion of polyanions. Here we use this free energy to describe a coacervate with non-optimal

structure. Since the structure of the complexes in this region is rather complicated and lies beyond the scope of this work, it will be described elsewhere. The qualitative behavior of the phase boundaries in this region is shown by the dashed line in Figure 11.

References

1. Zhao Q, Lee DW, Ahn BK, Seo S, Kaufman Y, Israelachvili JN, Waite JH “Underwater contact adhesion and microarchitecture in polyelectrolyte complexes actuated by solvent exchange”, Nature Materials 2016, 15, 407–412. [PubMed: 26779881]
2. de Kruif CG, Weinbreck F, and de Vries R, “Complex coacervation of proteins and anionic polysaccharides”, Curr. Opin. Colloid Interface Sci 2004, 9, (5), 340–349.
3. Weinbreck F, de Vries R, Schrooyen P, and de Kruif CG, “Complex coacervation of whey proteins and gum arabic”, Biomacromolecules 2003, 4, (2), 293–303. [PubMed: 12625724]
4. Luzzi LA, “Microencapsulation”, J. Pharm. Sci 1970, 59, (10), 1367–1376. [PubMed: 4919443]
5. Delcea M, Mohwald H, and Skirtach AG, “Stimuli-responsive LbL capsules and nanoshells for drug delivery”, Adv. Drug Delivery Rev 2011, 63 (9), 730–747.
6. Zhao H, Sun C, Stewart RJ, and Waite JH, “Cement Proteins of the Tube-building Polychaete Phragmatopoma californica”, J. Biol. Chem 2005, 280, (52), 42938–42944. [PubMed: 16227622]
7. Wei W, Tan Y, Rodriguez NRM, Israelachvili J Yu JN, and Waite JH, “A mussel-derived one component adhesive coacervate”, Acta Biomater. 2014, 10 (4), 1663–1670. [PubMed: 24060881]
8. Buriuli M and Verma D, “A mussel-derived one component adhesive coacervate”, Advances in Biomaterials for Biomedical Applications, Advanced Structured Materials 66, Springer Nature, Singapore, 45–93, 2017.
9. Kabanov V “Fundamentals of Polyelectrolyte Complexes in Solution and the Bulk”, In Multilayer Thin Films; Decher G., Schlenoff JB, Eds.; WILEI-VCH: Weinheim, Germany, 47, 2003.
10. Kabanov VA “Basic Properties of Soluble Interpolyelectrolyte Complexes Applied to Bioengineering and Cell Transformations”, In Macromolecular Complexes in Chemistry and Biology; Dubin P, Bock J, Davies RM, Schulz DN, Thies C, Eds.; Springer-Verlag: Berlin, Germany, 151, 1994.
11. van der Gucht J, Spruijt E, Lemmers M, Cohen Stuart MA, “Polyelectrolyte complexes: bulk phases and colloidal systems”, J. Colloid Interface Sci 2011, 361, 407–422. [PubMed: 21705008]
12. Priftis D, Tirrell M, “Phase behaviour and complex coacervation of aqueous polypeptide solutions”, Soft Matter 2012, 8, 9396.
13. Li L, Srivastava S, Andreev M, Marciel AB, de Pablo JJ, and Tirrell MV, “Phase Behavior and Salt Partitioning in Polyelectrolyte Complex Coacervates”, Macromolecules 2018, 51, 2988–2995.
14. Overbeek JT, Voorn MJ, “Phase separation in polyelectrolyte solutions; theory of complex coacervation”, J. Cell Physiol. Suppl 1957, 49, 7–22. [PubMed: 13449108]
15. Michaeli I, Overbeek J. Th. G., Voorn MJ, “Phase separation of polyelectrolyte solutions”, J. Polym. Sci 1957, 23, 443–450.
16. Borue VY, Erukhimovich IY, “A statistical theory of globular polyelectrolyte complexes”, Macromolecules 1990, 23, 3625–3632.
17. Castelnovo M, Joanny JF, “Complexation between oppositely charged polyelectrolytes: Beyond the Random Phase Approximation”, Eur. Phys. J. E 2001, 6, 377–386.
18. Kudlay A, Olvera de la Cruz M, “Precipitation of oppositely charged polyelectrolytes in salt solutions”, J. Chem. Phys 2004, 120, 404–412. [PubMed: 15267302]
19. Kudlay A, Ermoshkin AV, de la Cruz MO, “Complexation of Oppositely Charged Polyelectrolytes: Effect of Ion Pair Formation”, Macromolecules 2004, 37, 9231–9241.
20. Zhang R, Shklovskii BI, “Phase diagram of solution of oppositely charged polyelectrolytes”, Physica A 2005, 352, 216–238.
21. Perry SL and Sing CE, “PRISM-Based Theory of Complex Coacervation: Excluded Volume versus Chain Correlation”, Macromolecules 2015, 48, (14), 5040–5053.

22. Peng B, Muthukumar M, “Modeling competitive substitution in a polyelectrolyte complex”, J. Chem. Phys 2015, 143, 243133. [PubMed: 26723618]
23. Ou Z, Muthukumar M, “Entropy and enthalpy of polyelectrolyte complexation: Langevin dynamics simulations”, J. Chem. Phys 2006, 124, 154902. [PubMed: 16674260]
24. Lytle TK, Radhakrishna M, и Sing CE, “High Charge Density Coacervate Assembly via Hybrid Monte Carlo Single Chain in Mean Field Theory”, Macromolecules, 2016, 49 (24), 9693–9705.
25. Sing CE, “Development of the modern theory of polymeric complex coacervation”, Adv Colloid Interface Sci. 2017, 239, 2–16. [PubMed: 27161661]
26. Popov YO, Lee J, Fredrickson GH, “Field-theoretic simulations of polyelectrolyte complexation”, J. of Pol. Sci.: B: Pol. Phys, 2007, 45, 3223–3230.
27. Lee J, Popov YO and Fredrickson GH, “Complex coacervation: a field theoretic simulation study of polyelectrolyte complexation”, J. of Chem. Phys 2008, 128, (22), 224908. [PubMed: 18554054]
28. Delaney KT and Fredrickson GH, “Theory of polyelectrolyte complexation-Complex coacervates are self-coacervates”, J. of Chem. Phys 2017, 146, 224902. [PubMed: 29166038]
29. Dobrynin A and Rubinstein M, “Theory of polyelectrolytes in solutions and at surfaces”, Progress in Polymer Science, 2005, 30, 1049–1118.
30. De Gennes PG, Pincus P, Velasco RM, Brochard F, “Remarks on polyelectrolyte conformation”, Journal de Physique, 1976, 37 (12) 1461–1473.
31. Rubinstein M and Colby RH, “Polymer physics”. Oxford; New York: Oxford University Press, 2003.
32. Wang Z and Rubinstein M, “Regimes of Conformational Transitions of a Diblock Polyampholyte”, Macromolecules 2006, 39, 5897–5912.
33. Shusharina NP, Zhulina EB, Dobrynin AV, and Rubinstein M, “Scaling Theory of Diblock Polyampholyte Solutions”, Macromolecules 2005, 38, (21), 8870–8881.
34. Rumyantsev AM, Zhulina EB and Borisov OV, “Complex Coacervate of Weakly Charged Polyelectrolytes: Diagram of States”, Macromolecules 2018, 51, 3788–3801.
35. Dobrynin AV, Deshkovski A, and Rubinstein M, “Adsorption of polyelectrolytes at oppositely charged surfaces”, Macromolecules, 2001, 34, 3421–3436.
36. Thünemann AF, Müller M, Dautzenberg H, Joanny J-F, Löwen H, “Polyelectrolyte Complexes”, Adv. Polym. Sci 2004, 166, 113–171.
37. Dobrynin AV, Colby RH, and Rubinstein M, “Scaling Theory of Polyelectrolyte Solutions”, Macromolecules 1995, 28, (6), 1859–1871.
38. Smith WF, Hashemi J, “Foundations of Materials Science and Engineering” (4th ed.), McGraw-Hill, Boston 2006.
39. Kremer K, Grest GS, “Dynamics of entangled linear polymer melts: A molecular-dynamics simulation”, J. Chem. Phys 1990, 92, 5057–5086.
40. Hockney RW and Eastwood JW, “Computer Simulation Using Particles”, CRC Press, Adam Hilger, NY, 1989.
41. Schneider T and Stoll E, “Molecular-dynamics study of a three-dimensional one-component model for distortive phase transitions”, Phys. Rev. B, 1978, 17, 1302–1308.
42. Plimpton S, “Fast Parallel Algorithms for Short-Range Molecular Dynamics”, J. Comp. Phys 1995, 117, 1–19.
43. Grest GS, Kremer K, “Molecular dynamics simulation for polymers in the presence of a heat bath”, Phys. Rev. A 1986, 33, 3628–3631.
44. Berendsen HJC, Postma JPM, van Gunsteren WF, DiNola A, Haak JR, “Molecular dynamics with coupling to an external bath”, J. Chem. Phys 1984, 81, 3684–3690.
45. Higgins JS and Benoit HC, “Polymers and Neutron Scattering”, Oxford, NY, 1996.

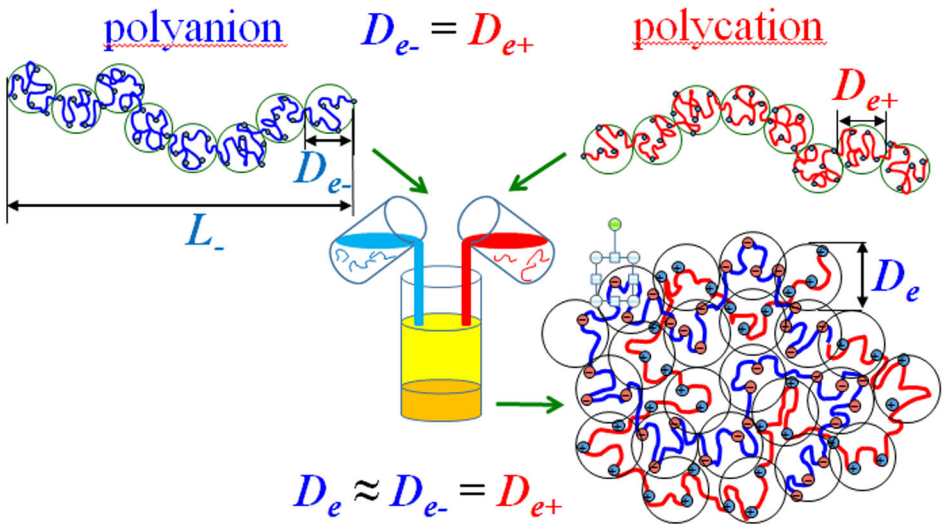

Figure 1.

Conformations of a polyanion and a polycation in dilute solutions (upper panels) and in a mixture of symmetric oppositely charged polyelectrolytes (lower panels).

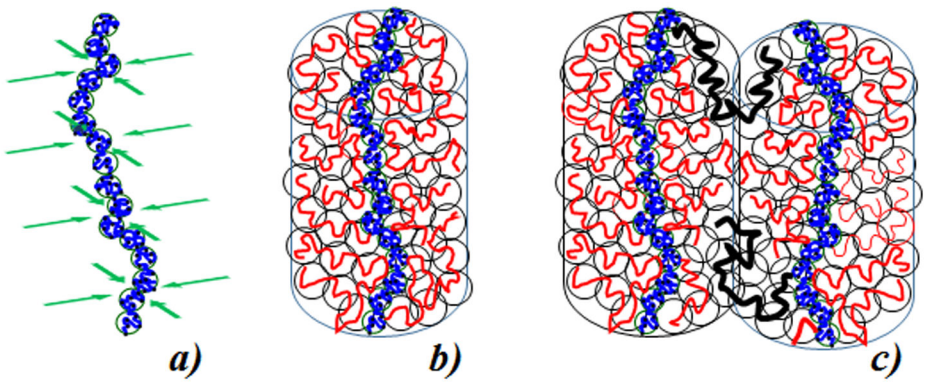

Figure 2.

a) The electric field (arrows show its lines) around the stronger charged polyanion attracts polycations. b) A polycation coat around a polyanion is stabilized by the steric repulsion between its monomers. c) The polycation coat of a polyanion is also electrostatically attracted to a neighboring polyanion. In addition, neighboring coats are stitched together in an asymmetric coacervate by bridges of polycation chains (thick black curves).

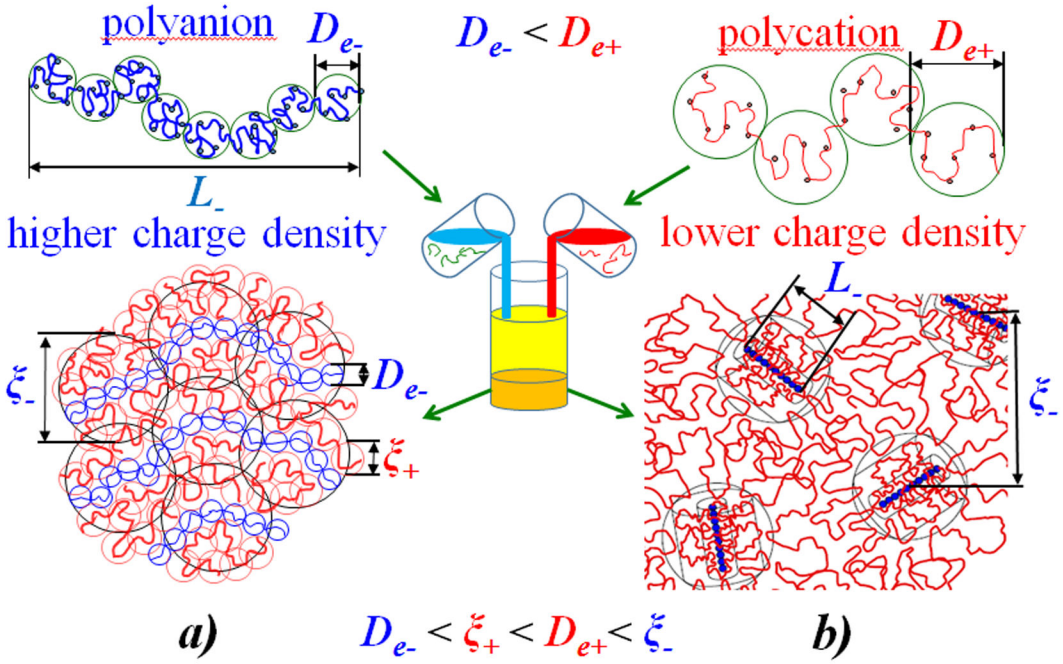

Figure 3.

Conformations of a polyanion and a polycation in dilute solutions and in a mixture of asymmetric oppositely charged polyelectrolytes: a) double-semidilute coacervate with $L_- > \xi_-$ and b) dilute-semidilute coacervate with $L_- < \xi_-$.

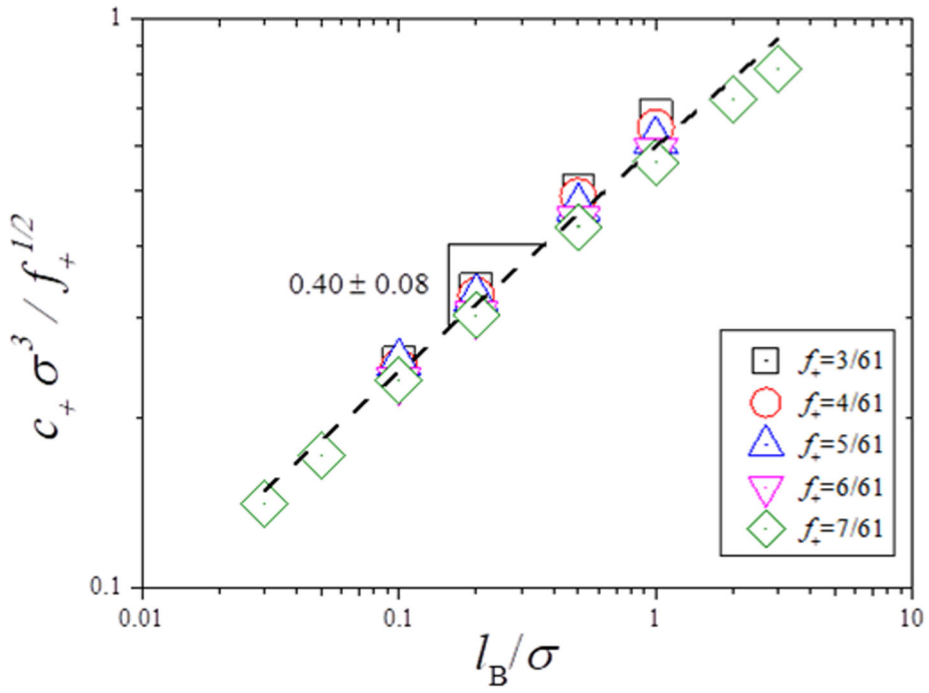

Figure 4.

Number density $\bar{c}_+$ of polycation monomers in a coacervate normalized by $f_+^{1/2}/\sigma^3$, where f_+ is the fraction of charged polycation monomers and σ is the Lennard-Jones length (Eq. 47 below), as a function of normalized Bjerrum length l_B/σ. Coacervates are formed by mixing polyanions containing $N_- = 101$ monomers per chain (fraction $f_- = 1/2$ of them charged) with polycations containing $N_- = 61$ monomers per chain and charge fraction f_+, as indicated in the figure legend.

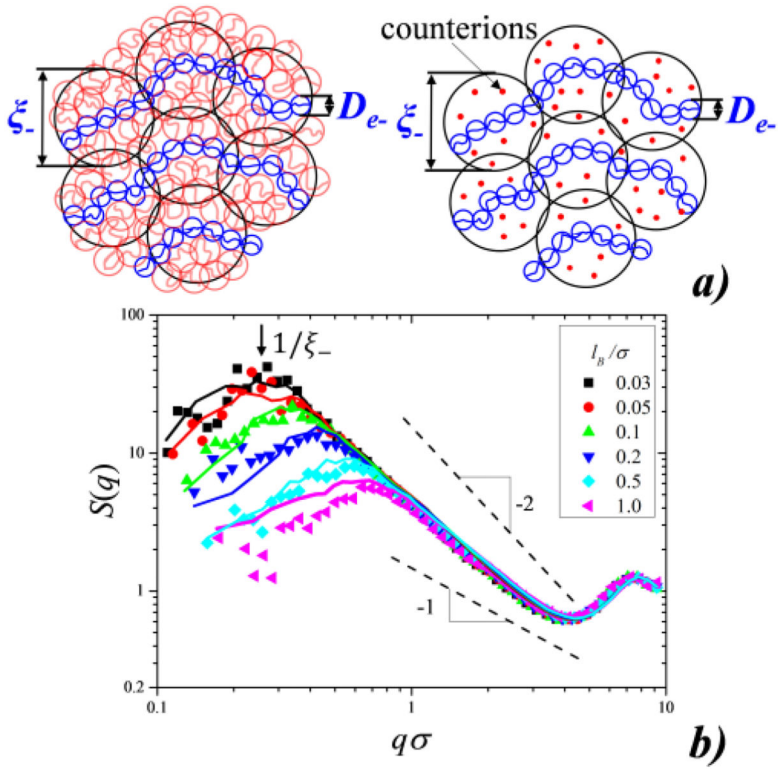

Figure 5.

a) Conformations of polyanions, shown by blue lines, in the coacervate (left) are analogous to their conformations in solutions of only polyanions (right) at the same concentrations. b) Comparison of the structure factors $S(q)$ of polyanions in coacervates (symbols) and in semidilute solutions (lines) with the same polyanion concentration $\bar{c}_-$ for various values of the Bjerrum length l_B. Polyanion chains contain $N_- = 101$ monomers each with charge fraction $f_- = 51/101$, while polycation chains contain $N_+ = 161$ monomers each with charge fraction $f_+ = 7/61$. See Eq. 50 below for the details of $S(q)$ calculation.

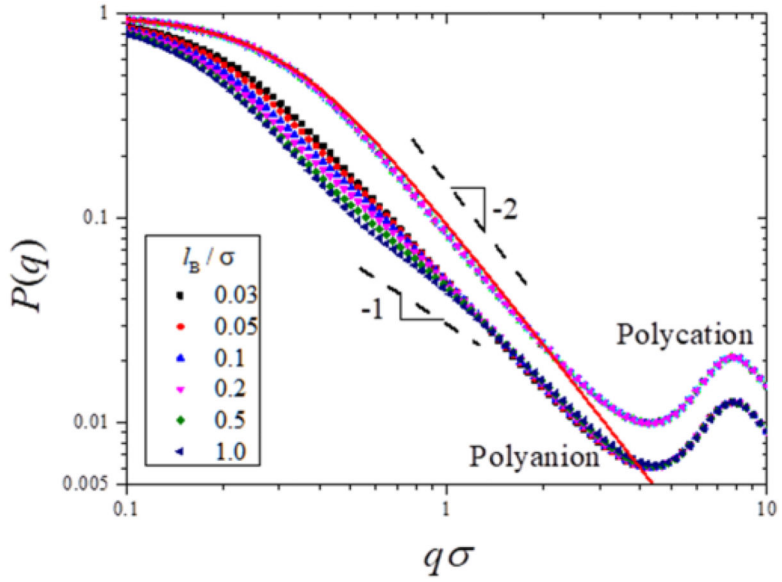

Figure 6.

Form factors (see Eq. 51 below) of polycations for different values of Bjerrum length l_B (upper sets of points, solid line is their best fit by the Debye function, see Eq. (52) below) with N_+ = 61 monomers per chain and charge fraction f_+ =7/61 and of polyanions (lower sets of points) with N_- = 101 monomers per chain and charge fraction f_- = 51/101.

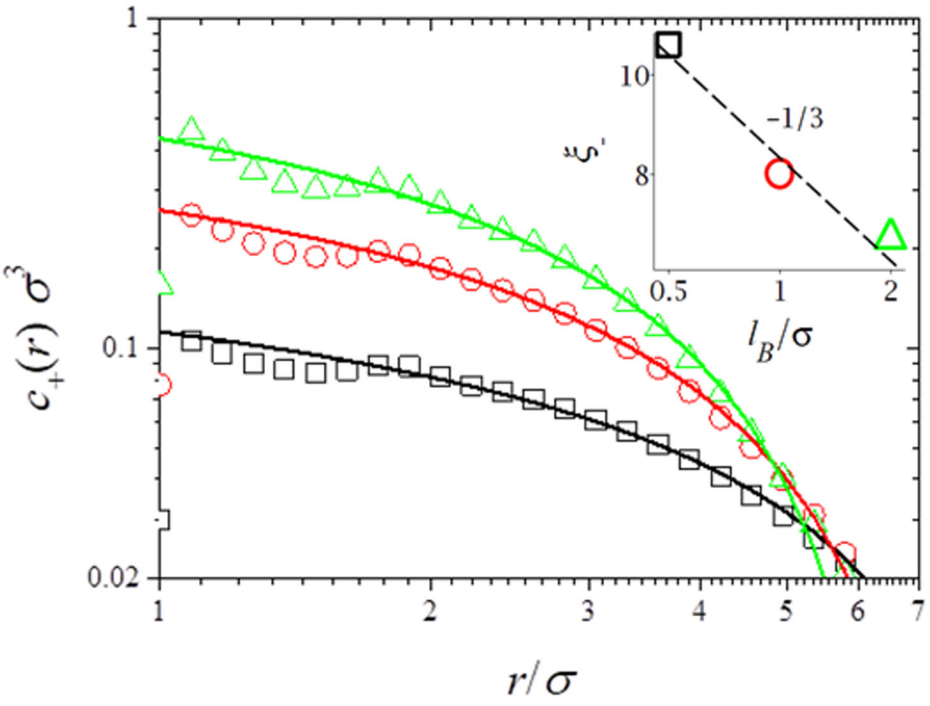

Figure 7.

The concentration profile $c_+(r)$ in polycation screening coat as a function of distance r from a polyanion rod with unit charge density $f_- = 1$. The fraction of polycation charge monomers is $f_+ = 0.07$. Different symbols correspond to different values of the Bjerrum length l_B. The solid lines are best fits to the data by equation 27 in the distance range $2\sigma < r < 6\sigma$. The fitting parameters are listed in Table 1. The resulting dependence of ξ_- on l_B/σ (symbols) and its theoretical prediction $\xi_- \sim (l_B/\sigma)^{-1/3}$ (dashed line) are shown in the inset.

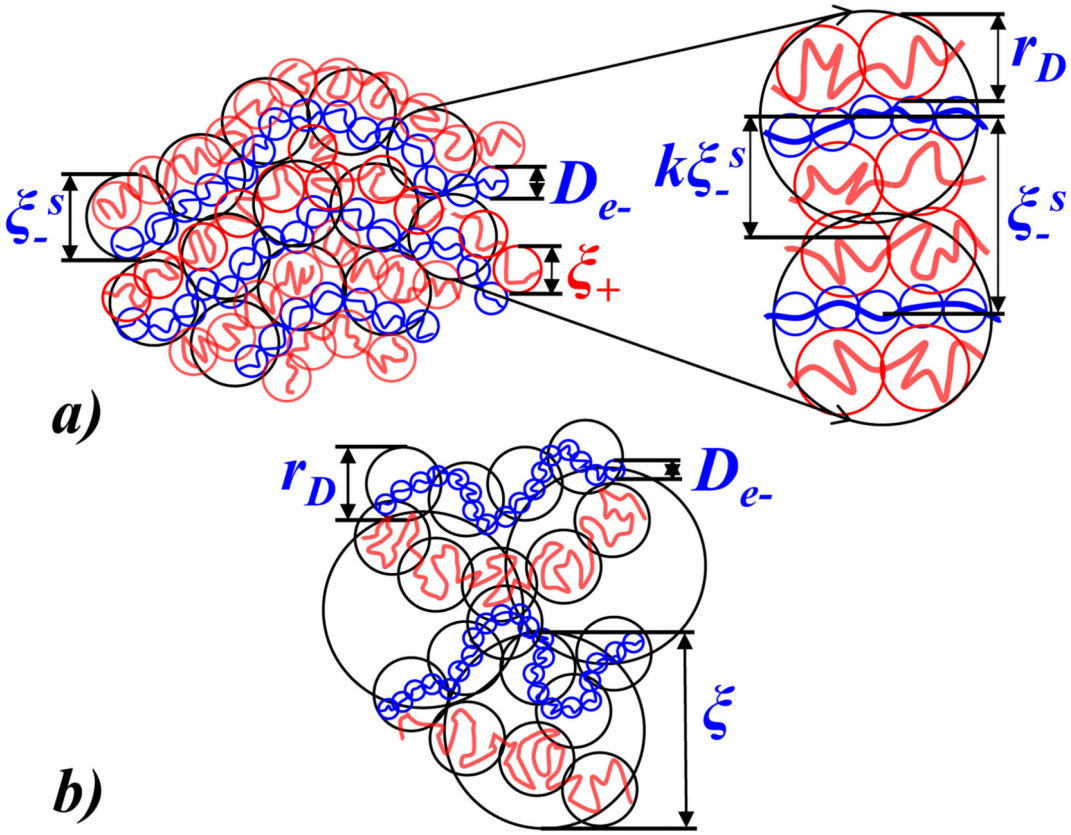

Figure 8.

Charged chain conformations in asymmetric coacervate with long polyanion chains $L_- > \xi_-$ at salt concentrations: a) $c_{s,l} < c_s < c_{s,h}$ in the intermediate salt regime with $\xi_+ < r_D < \xi_-$ and b) $c_s > c_{s,h}$ in the high salt regime with $r_D > \xi_+$.

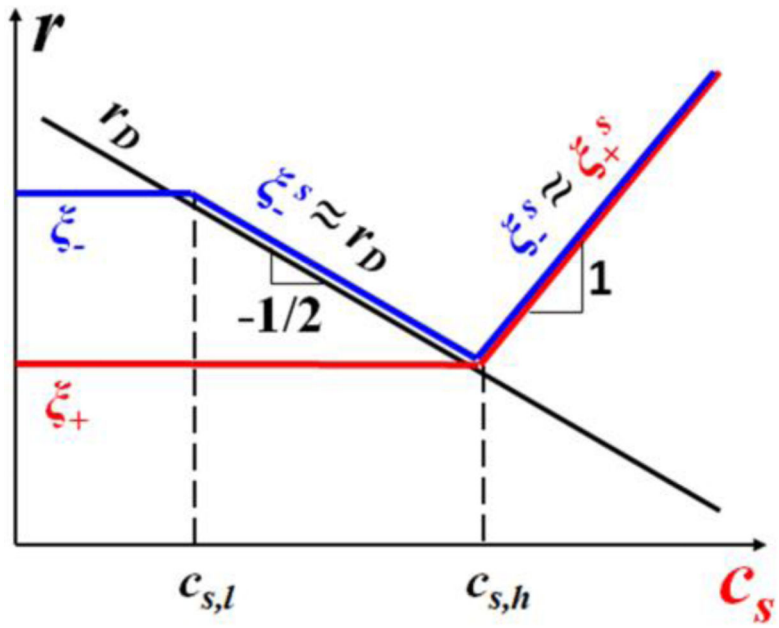

Figure 9.

Salt concentration dependence of the Debye length r_D (solid black line), polyanion correlation length ξ_-^s (solid blue line), and polycation correlation length ξ_+^s (solid red line) in an asymmetric coacervate with long polyanion chains, $L_- > \xi_-$.

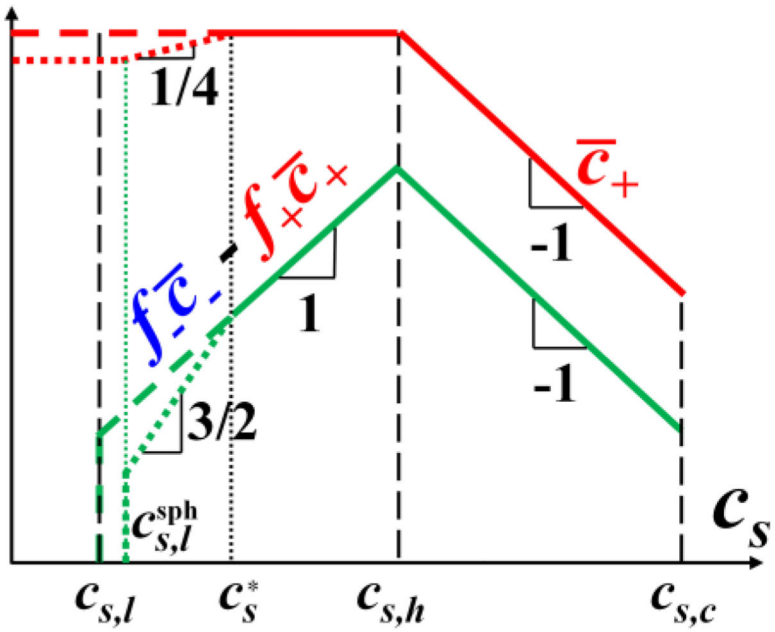

Figure 10.

Salt concentration dependence of the coacervate concentration $\bar{c} \simeq \bar{c}_+$ (red lines) and number density of charges on chains $f_-\bar{c}_- - f_+\bar{c}_+$ (green lines) in the optimal asymmetric coacervate (log-log scales). Dashed and dotted lines correspond to longer and shorter polyanions with $L_- > \xi_-$ and $c_s^* < c_{s,l}$ and $L_- < \xi_-$ and $c_s^* > c_{s,l}$, respectively.

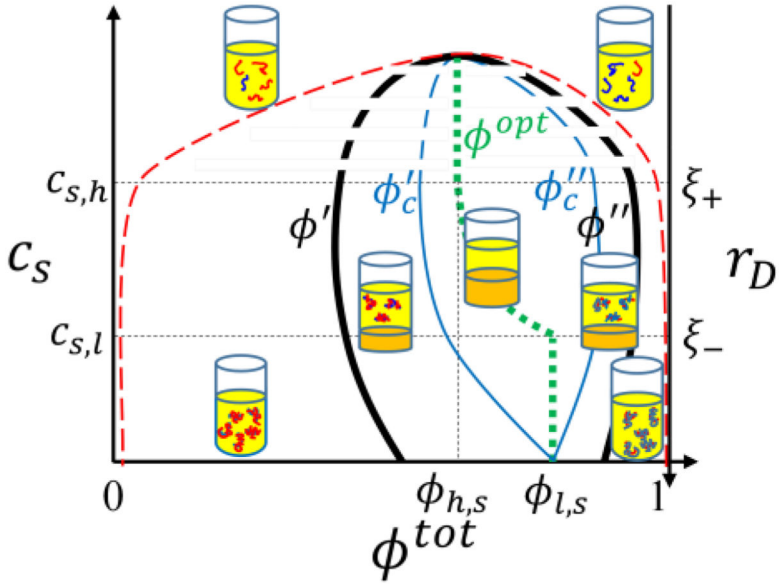

Figure 11.

Phase diagram of a mixture of oppositely charged weakly interacting polyelectrolytes. The horizontal axis is the number fraction of polycation monomers in solution $\phi^{tot} = \bar{c}_+^{tot}/(\bar{c}_+^{tot} + \bar{c}_-^{tot})$. The left vertical axis is salt concentration c_s, whereas the right vertical axis (pointing down) is the corresponding Debye length. The thick black lines (ϕ' and ϕ'') are the phase boundaries between two-phase region, containing coacervate (denoted by orange sediment in cartoons) and single-phase regions, containing dilute chains, denoted by red and blue lines and complexes containing chains of both signs. The complexes exist only in regions between outside thin blue lines (ϕ_c' and ϕ_c'') and inside red dash lines. The green dotted line (ϕ^{opt}) corresponds to the optimal coacervate composition.

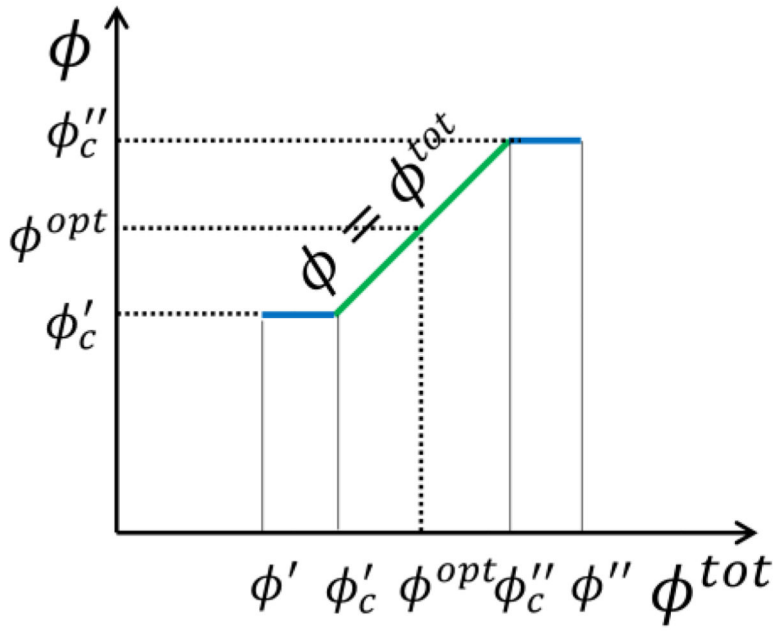

Figure 12.

The dependence of the number fraction of polycation monomers ϕ in the coacervate on total number fraction ϕ^{tot} in the mixture.

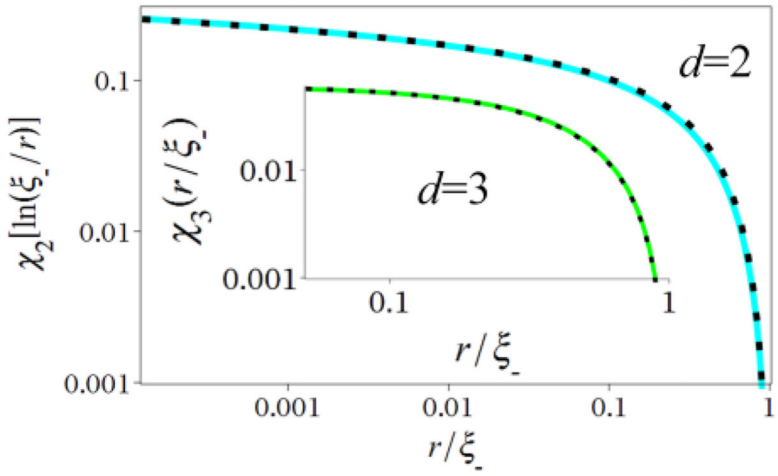

Figure 13.

Numerical solution for the concentration profile $c_+(r) \sim \chi_2[\ln(\xi_-/r)]$ (solid line) in the salt-free regime for $d = 2$, and its approximation by Eq. (B6) (dotted line). Inset: numerical solution for the function $\chi_3(r/\xi_-)$ (solid line) and its approximation by Eq. (B6c) (dotted line) in the case of spherical symmetry $d = 3$.

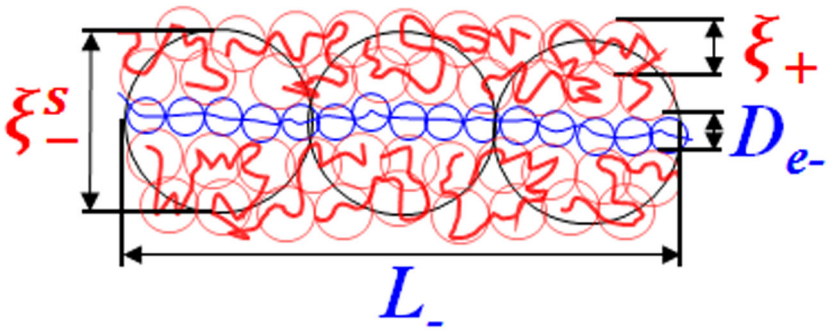

Figure 14.
Cylindrically-shaped complex

Table 1.

Average concentration $\bar{c}_+$ of polycations and correlation length ξ_- of polyanions obtained from the fits of Eq. (27) to the simulation data presented in Figure 7.

l_B/σ	$\bar{c}_+$ [σ^{-3}]	ξ_- [σ]
0.5	0.089 ± 0.002	10.7 ± 0.2
1.0	0.233 ± 0.004	8.02 ± 0.11
2.0	0.410 ± 0.008	6.94 ± 0.09